Review of Electromagnetic Techniques for Breast Cancer Detection

Ahmed M. Hassan, *Student Member, IEEE*, and Magda El-Shenawee, *Senior Member, IEEE*

Methodological Review

***Abstract*—Breast cancer is anticipated to be responsible for almost 40,000 deaths in the USA in 2011. The current clinical detection techniques suffer from limitations which motivated researchers to investigate alternative modalities for the early detection of breast cancer. This paper focuses on reviewing the main electromagnetic techniques for breast cancer detection. More specifically, this work reviews the cutting edge research in microwave imaging, electrical impedance tomography, diffuse optical tomography, microwave radiometry, biomagnetic detection, biopotential detection, and magnetic resonance imaging (MRI). The goal of this paper is to provide biomedical researchers with an in-depth review that includes all main electromagnetic techniques in the literature and the latest progress in each of these techniques.**

***Index Terms*—Biomagnetic detection, biopotential detection, breast cancer, diffuse optical tomography, electrical impedance tomography, magnetic resonance imaging (MRI), microwave imaging, microwave radiometry.**

I. Introduction

ACCORDING TO the American Cancer Society, 230,480 women are anticipated to be diagnosed with breast cancer in the U.S. in 2011 alone [1]. This number is larger than any other kind of cancer in females and accounts for almost 30% of the total estimated new cancer cases for women. Additionally, 39,520 breast cancer related deaths are expected in the U.S. in 2011. These statistics clearly demonstrate the gravity of this disease and its impact on the health and welfare of society.

Since the 1960s, studies have been performed to test the hypothesis that regular screening for breast cancer can reduce the mortality rate of this disease [2]. The primary screening method has been X-ray mammography, which is currently the golden standard for breast cancer screening [2]. The important conclusion of these studies is that early detection of breast cancer significantly improves the outcome of treatment and reduces the mortality rate which justifies regular screening [2]–[4]. However, the recent recommendation of the U.S. Preventive Services Task Force (USPSTF) to start screening using mammography at the age of 50 instead of the age of 40 has been the subject of serious controversy [5]. Moreover, there is a debate on the extent of benefit of screening using X-ray mammography [6]. However, there is a general consent that regular screening of breast cancer should be performed, especially for women between the ages of 50 and 74 years [5].

The limitations of the X-ray mammography method present a significant challenge to the accurate detection of breast cancer. These limitations are behind the motivation to develop alternative detection techniques. However, the current clinical alternatives to X-ray mammography still suffer from their own challenges which will be discussed in the next section. The goal of this paper is to provide an up-to-date review of the research performed using electromagnetic detection methods. The following modalities are reviewed herein: microwave, electrical impedance tomography (EIT), diffuse optical tomography (DOT), microwave radiometry, biopotential, biomagnetic and magnetic resonance imaging (MRI).

To the best of our knowledge there have been only two papers that reviewed electromagnetic modalities of breast cancer detection, [7] and [8]. The current review paper presents an update of the extensive research in the literature since publishing [7] and [8]. In addition, other electromagnetic methods for breast cancer detection are added in this review paper. A brief review of the different electromagnetic modalities was presented in [9].

The modalities reviewed herein, microwave, electric impedance tomography, diffuse optical tomography, microwave radiometry, biopotential and biomagnetic, have similar features and are reviewed under the subtitles: Physical Quantity Sensed, Imaging Systems, Imaging Algorithms (or numerical modeling), and Clinical Trials. The biomagnetics section is included for completeness as it represents preliminary work with few published papers. MRI also belongs to the spectrum of electromagnetic techniques, but it has different features. The MRI is a more advanced technique and, therefore, its section is focused on clinical applications for breast cancer detection.

II. Limitations of Current Breast Cancer Detection Techniques

Currently, the standard technique for breast cancer screening and detection is X-ray mammography. Yet the rate of failure of mammography in detecting breast cancer, termed false negative, is relatively high and ranges from 4% to as high as 34% [10]. The ionizing X-ray in mammography poses a serious health risk

Manuscript received December 06, 2010; revised June 28, 2011; accepted September 13, 2011. Date of publication September 29, 2011; date of current version January 06, 2012. This work was supported in part by the National Science Foundation EDA under Award 0965571 (2010 Advances in Breast Cancer Research Workshop) and the Doctoral Academy Fellowship at the University of Arkansas.

The authors are with the Department of Electrical Engineering, University of Arkansas, Fayetteville, AR 72701 USA (e-mail: amhassan@uark.edu; magda@uark.edu).

Digital Object Identifier 10.1109/RBME.2011.2169780

TABLE I
COMPARISON OF PERFORMANCE OF DIFFERENT BREAST CANCER DETECTION TECHNIQUES [15]

Modality	Sensitivity	Specificity	Positive Predictive Value	Accuracy
Mammography	67.8% (120/177)	75% (61/81)	85.7% (120/140)	70.2% (181/258)
Mammography and clinical examination	77.4% (137/177)	72% (58/81)	58.6% (137/160)	75.6% (195/258)
Clinical examination	50.3% (89/177)	92% (75/81)	94% (89/95)	63.6% (164/258)
Ultrasound	83.0% (147/177)	34% (28/81)	73.5% (147/200)	67.8% (175/258)
Mammography and Ultrasound	91.5% (162/177)	23% (19/81)	72.3% (162/224)	70.2% (181/258)
Mammography, clinical examination, and Ultrasound	93.2% (165/177)	22% (18/81)	72.4% (165/228)	70.9% (183/258)
MRI	94.4% (167/177)	26% (21/81)	73.6% (167/227)	72.9% (188/258)
Mammography, clinical examination, MRI	99.4% (176/177)	7% (6/81)	70.1% (176/251)	70.5% (182/258)

to women and can even increase the chance for cancer development [11], [12]. An alternative technique for breast cancer detection is the MRI; it offers higher sensitivity but at a tradeoff with high cost and low specificity which can lead to over diagnosis [13],[14]. Therefore, MRI is not currently used for breast cancer screening except for high risk cases [13], [14]. Ultrasound (US) has also been utilized in breast cancer detection with a false negative rate of 17% [15].

In order to improve breast cancer detection, combining different detection modalities has been investigated in [15]. This study involved 258 patients, 177 patients with malignant tumors and 81 with benign tumors [15]. Four parameters were used to test each detection technique: sensitivity, specificity, positive predictive value, and accuracy. Sensitivity is defined as the ratio of malignant tumors detected to the total number of patients with malignant tumors. Specificity is defined as the ratio of patients correctly classified as having benign tumors to the total number of patients with benign tumors. The positive predictive value is the ratio of the number of patients correctly diagnosed to have malignant tumors to the total number of positive diagnoses. The total number of positive diagnoses consists of patients with malignant tumors correctly diagnosed as positive in addition to patients with benign tumors incorrectly diagnosed as positive. Finally, accuracy is the ratio of the number of patients correctly diagnosed, whether they have benign or malignant tumors, to the total number of patients.

A summary of the results obtained in [15] is presented in Table I which shows the number of correct diagnoses in each category as well as the percentage. The highest sensitivity, 99.4%, was achieved when mammography, clinical examination, and MRI were combined. However, in this case the specificity dropped to only 7%. The maximum accuracy obtained from any combination was 75.6% which means that one diagnosis is wrong in every four diagnoses. Therefore, a combination of the current detection modalities is not sufficient to enhance the accuracy, reduce the cost, increase the safety, and reduce the discomfort of breast cancer detection.

The previous statistics show that the current clinical techniques suffer from limitations for breast cancer detection. These limitations motivated researchers globally to investigate new alternative detection techniques substantially different from the techniques presented in Table I. In particular, electromagnetic (EM) detection techniques have been receiving rising interest in recent years. The EM detection of breast cancer relies on: 1) the presence of a contrast in the electromagnetic properties between breast and tumor tissues; 2) the unique electrical signals generated by cancerous cells; or 3) the nuclear magnetic resonance (NMR). The next sections will review the progress in different EM breast cancer detection techniques.

III. MICROWAVE IMAGING

A. Physical Quantity Sensed

Microwave imaging of breast cancer has received extensive attention lately. The main motivation was the hypothesis that the electrical properties, permittivity and conductivity, of malignant breast tumors tissue differ significantly from those of the normal surrounding breast tissue. The difference was estimated to be almost five to ten times larger [7]. Also, microwave frequencies are nonionizing and exhibit reasonable penetration in breast tissue, although with moderate to low resolution. In microwave imaging, the sensors are the transmitter and receiver antennas. The transmitter antennas illuminate the breast with microwave signals and the signals scattered back from the breast are collected by the receiver antennas. Cancerous tissues have dielectric permittivities and conductivities that are different than those of healthy breast tissues. Therefore, when an incident wave is exerted, cancerous tissue will scatter differently indicating their presence. Microwave imaging has been employed in few clinical trials and it exhibited a minimum detected tumor size of 5–10 mm, and a preliminary accuracy of 80%–90% [16]. The following subsections review the recent progress in the key components of microwave imaging of breast cancer.

B. Imaging Systems

The first near-field microwave imaging system used in clinical trials was developed at Dartmouth College by Meaney *et*

al. [17]. The system consisted of a circular antenna array of 32 monopoles operating in the frequency range 300–1000 MHz. The antenna array was positioned in a tank filled with saline to act as the coupling medium between the antennas and the breast. The patient lay in the prone position with her breast hanging, through an opening in the table, into the tank where the antennas were immersed. The antenna array moved vertically, in 1-cm steps, through a mechanical jack to acquire measurement from the chest level down to the nipple. A microwave switching system was used to select which antenna transmits the power from the microwave source and which antenna sends its received power to the receiver.

Another ultra-wideband microwave imaging system was developed by Klemm *et al.* at the University of Bristol [18]. In comparison to the system of Meaney *et al.*, this system operated at higher frequencies (4.5–10 GHz) which were achieved by employing cavity-backed patch antennas instead of monopole antennas. Furthermore, Klemm *et al.* employed a 3-D hemispherical antenna array versus the 2-D circular array by Meaney *et al.*

In addition to the development of complete systems, extensive research was performed to advance the antennas, which are the sensors for the microwave imaging modality [19]–[27]. Desired characteristics of these antennas were ultra-wideband, compact size, steerable, dual independent linear polarization, isolation from nearby interference, and high radiation efficiency [19]–[27]. Several antenna types have been proposed such as dipole antennas [19], dielectric resonator antennas [20], patch antennas [21], [22], slot antennas [22], Vivaldi antennas [23], Horn antennas [24], [25], and MEMS-steerable antennas [26], [27].

Most of the previously mentioned antennas require a matching liquid to reduce the mismatch between the antenna and the skin layer. However, the Horn antenna in [25] was augmented with a dielectric enclosure such that it does not require a matching liquid which reduced the complexity of the imaging system. In [23], the conventional Vivaldi antenna was augmented with a high permittivity dielectric material, director, to focus the power of the antenna more effectively into the region of interest. This director had the effect of increasing the scattered energy received from the tumor [23]. A comparison between wide-slot antennas and stacked patch antennas for microwave breast imaging was performed in [22]. Even though the two antennas operated at the same frequencies, the wide-slot antenna was found to be three times smaller than the stacked-patch which could allow the integration of larger arrays of antennas in the microwave imaging system [22]. The comparison in [22] can be the basis of future comparisons in order to identify the optimum antenna for the microwave imaging of the breast. The MEMS-steerable antenna in [26] and [27] was designed on a platform which can rotate in two dimensions and, therefore, can enhance the efficiency of scanning different areas in the breast. Another advantage of the antennas in [26] and [27] was their capability of generating two independent linear polarizations. Testing two linear polarizations during the microwave imaging of the breast was found to be advantageous since it was shown that likelihood of detecting the tumor increases if the polarization of the incident wave was along the major axis of the tumor [28].

C. Imaging Algorithms

A healthy breast is generally composed of an outer skin layer, fatty tissue, and fibroglandular tissue. The fibroglandular tissue is composed of the ducts and lobules inside the breast. One of the first steps in microwave imaging of the breast is reconstructing the outer shape of the breast [29], [30]. Identifying the outer surface of the breast can improve the accuracy and the speed of the consequent steps of imaging the interior of the breast [29]. In addition, the skin layer reflects a considerable portion of the incident microwaves even when a matching liquid between the microwave sources and the breast was utilized [31]. By identifying the outer surface of the breast, the effect of the skin layer can be removed from the signature of the internal structures such as the tumor [31]. In the algorithm proposed in [29], the first step involved reconstructing a number of points on the breast surface equal to the number of antennas used in the imaging. Those points were then interpolated and extrapolated to achieve a larger number of points. Finally, these points were used to generate surface functions to estimate the smooth continuous surface of the breast [29]. Current breast surface identification techniques were successful in reconstructing the surface of the breast within an error of few millimeters [29], [30].

There are two main modalities for imaging the interior of the breast: 1) microwave tomography [17], [32]–[35] and 2) radar-based imaging [36]–[43]. In microwave tomography, a reconstruction of the electrical properties of the breast at each pixel was calculated [17], [32]–[35]. On the other hand, in radar-based imaging signal processing techniques were employed to identify regions of strong backscatter similar to conventional radars. The regions of large backscatter indicated the presence of a contrast in electrical properties such as the contrast between cancerous and healthy tissue [36]–[43]. The shape of the tumor is one of the key parameters to be reconstructed in microwave imaging of the breast [44]. The importance of the tumor shape lies in the fact that benign tumors tend to have a round smooth shape whereas malignant tumors tend to have irregular nonsymmetrical shapes [44]. Therefore, detecting the shape of the tumor can help diagnose it as malignant or benign. Reconstructing the shape of the tumor was achieved in [44] using the spherical harmonics expansion. The optimum spherical harmonic coefficients to reconstruct the shape of the tumor were obtained through a gradient descent optimization method combined with a forward solver [44]. An updated algorithm for the shape reconstruction of the tumor, based on the hybridization of the adjoint-field scheme with the method of moments, was presented in [45]. The adjoint-field algorithm allowed the update of each node on the surface of the evolving object during the reconstruction without any parameterization. By updating each surface node, the adjoint-field algorithm allowed the reconstruction of a larger family of tumor shapes [45].

A different imaging modality was developed in [46]. The method involves measuring the resonance spectra from the breast. Tumors were found to resonate at unique frequencies independent of the incident polarization, direction, or tumor depth. The resonance of the tumor was found to depend only on the tumor shape and dielectric properties [46].

D. Clinical Trials

The system developed by Meaney *et al.* was used in clinical trials in [16] and [47]. In [16], the system was used to image the breasts of 43 healthy patients with no tumor. The study revealed two important conclusions. The first conclusion was the high correlation between the average electrical properties in the microwave region in both breasts [16]. The second was the increase in the average and local electrical properties in the microwave region with the increase in radiographic breast density. The radiographic breast density is defined as the amount of fibroglandular tissue relative to the amount of fat in the breast [16].

The clinical trial in [47] tested the microwave imaging system on 80 patients with abnormal mammograms and 50 patients with normal mammograms. The electrical permittivity and conductivity in the region of interest (ROI), the region which was suspicious in the mammogram, were reconstructed using the measured microwave data. The electrical permittivity and conductivity in the ROI were then compared to the background permittivity and conductivity outside the ROI in the ipsilateral breast (the breast with the suspicious legion) and to the mirrored ROI in the contralateral breast (the other breast). In the normal patients pseudo-ROI were selected. The results showed that cancerous tumors more than 1 cm in diameter exhibited twice as large conductivity in comparison to the background tissue. This ratio was statistically larger than that of benign tumors or that exhibited by healthy patients [47].

The system developed by Klemm *et al.* was used in preliminary clinical trials in [48]. The microwave imaging system provided qualitative agreement with the images obtained by X-ray mammography for certain patients.

E. Tissue Electrical Properties Measurements

In a large scale study performed by Lazebnik *et al.* at the University of Wisconsin and the University of Calgary in 2007, the dielectric properties of normal, benign, and malignant tissue were measured *ex vivo* [49], [50]. The study involved 354 normal breast tissue specimens from healthy patients (breast reduction) and 319 tissue specimens from cancer surgeries over a frequency range from 0.5 to 20 GHz. The normal breast tissue was divided into three groups: 1) 0%–30%; 2) 31%–84%; and 3) 85%–100% adipose (fat) tissue content. The frequency variation of the measured complex permittivity of each tissue type was then represented accurately using a one pole Cole–Cole model [49], [50]. Representing the dispersive properties of the biological tissue using the Cole–Cole or Debye models can simplify microwave tomography because only the parameters of the Cole–Cole or the Debye model need to be reconstructed instead of reconstructing a different permittivity value at each frequency [51].

The main conclusions of the study were that the dielectric properties of normal breast tissue heavily depend on the adipose percentage. Also, it was concluded that the dielectric properties of normal breast tissue exhibit a large variation in the microwave range. More importantly, the contrast in dielectric properties between malignant tumor tissue and adipose dominated tissue was as high as 10:1 [49], [50]. However, the contrast in dielectric properties between malignant tumor tissue and normal low adipose (fibroglandular) tissue was found to be $\sim$10%. The later finding implies that the signature of the tumor is significantly reduced in younger women where the fibroglandular portion of the breast is significant. However, in older women the fibroglandular portion of the tissue is considerably reduced and, therefore, it is anticipated that microwave imaging has more potential in older women than in younger women [28]. The unexpected conclusion of the low contrast in the electrical properties of malignant tumors with respect to the surrounding breast tissue represented a setback for the microwave imaging of breast cancer.

A different study by Halter *et al.* [52] indicated that the measurements performed by Lazebnik *et al.* were performed *ex vivo* and did not consider the variation in the dielectric properties of breast tissue *in vivo*. However in [52], the difference in the dielectric properties between *in vivo* and *ex vivo* was in the range of 20% to 39% depending on the frequency. This small difference is not convincing to justify the significant contrast between cancerous and healthy tissue originally assumed in the microwave region [7].

Two approaches were developed to overcome the low contrast limitation: 1) using a hybrid imaging modality [53], [54] and 2) using contrast agents in the microwave range [55]–[58]. Examples of the hybrid imaging modality is a scheme which combines microwave with acoustic imaging [53] or microwave with MRI [54]. The first scheme aimed to combine the contrast in dielectric properties in the microwave region with the contrast in elastic properties between cancerous and healthy tissue. The concept of the hybrid modality in [53] was to exert low frequency acoustic signals to induce displacements in the breast tissue, which were displaced according to their elastic properties. The microwave signals were then exerted on the breast where the scattered microwave signals were modulated by the displacement caused by the acoustic signals [53]. Upon combining acoustic and microwave imaging methods, the harmonic backscatter signature from the tumor was increased by $\sim$4.5 dB [53].

In the second hybrid modality, microwaves were integrated with MRI to develop magnetic resonance microwave absorption (MRMA) [54]. The concept of MRMA was to exert microwave pulses on the breast, with different biological tissues absorbing different amounts of the incident waves. The expansion of the different tissues led to different displacements which were detected as phase contrasts in the MRI [54]. In the feasibility study performed by Xie *et al.* the expansion displacements, due to microwave absorption, were successfully detected using MRI [54].

As for the contrast agent approach, microbubbles [55] and carbon nanotubes [56] were tested as contrast agents in the microwave region. The purpose of the imaging technique augmented with contrast agents was to perform two measurements and two reconstructions, one before administering the contrast agent and one after administering the contrast agent [57]. A breast phantom composed of ethylene glycol was found to have $\sim$50% lower permittivity and $\sim$60% lower conductivity with 30% of its weight composed of microbubbles in comparison to pure ethylene glycol at 3 GHz [55]. In [56], a tissue phantom with 0.22% of its weight composed of carbon nanotubes was

found to have ∼37% higher permittivity and ∼81% higher conductivity in comparison to the same phantom with no nanotubes. These differences in the dielectric properties were incorporated with an imaging algorithm to test whether the addition of the contrast agents benefit the detection of breast tumors or not [57]. Even though this approach was successful in detecting the tumors in [57], it required a relatively high signal-to-noise ratio (SNR) ∼40 dB. Another factor worth consideration is that the contrast agent can diffuse inside the tumor and therefore could distort the tumor shape in comparison to the precontrast stage as mentioned in [58].

Biocompatibility and safety of contrast agents are significant factors in determining the efficacy of their use. Microbubbles filled with gas have been heavily employed in ultrasound and they are safe as long as the amount of injected gas does not exceed 200 μL [59], [60]. It is also necessary to use pharmaceutically safe materials for the coating and the enclosed gas to ensure the biocompatibility of the microbubbles, e.g., cross-linked serum albumin, spray-dried serum albumin and phospholipids for the coating and air, octafluoropropane, and perfluorocarbon gas for the enclosed gas [60]. In the administration of microbubbles, special care has to be taken such that the bubbles do not block blood capillaries and cause microembolism [60]. Typical concentrations of intravenously administered microbubbles are around 10^9 microbubbles/mL and their sizes are typically less than 8 μm.

As for single wall carbon nanotubes (SWCNT), there have been several studies testing their biocompatibility using animals and human cell line [61]. The reported controversy in the level of SWCNT cytoxicity can be explained by the contamination with metallic residue during fabrication that can induce cytoxic effects [61]. Several studies showed that highly soluble SWCNT, which are less likely to form agglomerates, are less toxic than SWCNT with lower solubility [61].

In summary, the use of contrast agents for microwave imaging is still an emerging topic with several challenges such as sensitivity and biocompatibility.

IV. Electrical Impedance Tomography (EIT)

A. Physical Quantity Sensed

In electrical impedance tomography (EIT), a 2-D or 3-D reconstruction of the impedance of the breast is created over the range of frequency from 100 Hz to ∼1 MHz [8], [62]. This is a lower frequency range than the one employed in the microwave imaging technique. EIT is accomplished by placing sensors on the surface of the breast with each sensor applying a current and then measuring the resulting voltage differences across the sensors. In some versions of EIT, a voltage was applied and the generated currents were measured [63]. The sensors employed in EIT are typically electrodes of square metallic patches [64] or silver/silver chloride electrodes [62]. By applying suitable reconstruction algorithms, the impedance of the breast could be reconstructed using the applied currents and the measured voltages [8]. Due to the differences between the permittivity and conductivity of cancerous and healthy tissue in the frequency range less than 1 MHz, tumor regions have different complex impedances compared to the surrounding healthy tissue.

B. Imaging Systems

Currently, the TransScan T-Scan 2000 is the only commercial impedance-based system approved by the Food and Drug Administration (FDA) [8]. However, it was approved to be used in association with X-ray mammography and not independently [8]. The system consists of a probe composed of a 8×8 planar electrode array and a handheld reference electrode [8], [62]. The patient lies on her back in the supine position such that the breast is as flat as possible. The probe is then scanned over the breast and the induced currents, magnitude and phase, are measured at different positions on the breast. The applied voltages range between 1 and 2.5 V [8], [62]. A 2-D map of the total impedance beneath the scan area is then generated in real time where tumors appear as bright spots on a computer screen due to their higher conductivity [8]. The TransScan imaging modality is termed electrical impedance scanning (EIS) since no complex reconstruction algorithms were employed and only small numbers of electrodes were utilized [65]. In case of a suspicious mammogram, a positive EIS detection will corroborate that the tumor is malignant and therefore a biopsy would be scheduled. However, a negative EIS detection meant that further tests were required [8]. The TransScan system suffers from the limitation that artifacts due to interfering muscles and bones could appear in the impedance map and also the maximum reliable imaging depth is ∼3.5 cm.

Another impedance based system, which received the Conformité Européenne (CE) mark in 2007, but is still pending for FDA approval is the mammograph electrical impedance komputer (MEIK) system. The system is composed of 256 electrodes arranged in a planar array, has a maximum imaging depth of ∼6 cm and provides pseudo-3-D reconstruction by constructing the impedance at seven 2-D planes of different depth in the breast [8], [66], [67]. The MEIK performs EIT using a large number of electrodes and complex reconstruction algorithms which image the impedance at different depths [65]. In each of the seven reconstruction planes, the resolution of the reconstructed impedance is ∼8 mm [66]. The smallest reconstructed tumors in clinical experiments had diameters ranging between 3–5 mm [8]. Similar to other EIT systems, the MEIK system faces difficulty in detecting tumors close to the breast nipple [8].

Researchers at the Rensselaer Polytechnic Institute developed the Adaptive Current Tomograph (ACT) system which can perform a simultaneous combination of 3-D EIT and 3-D X-ray reconstruction [63]. This combination was achieved by employing electrodes for EIT that were transparent to X-rays. The simultaneous reconstruction using both modalities allowed for an accurate comparison without any fear of changing the breast position and consequently the breast profile [63]. The system was employed in preliminary clinical trials [64].

The contact pressure between each electrode and the breast is one of the most serious challenges of EIT for breast cancer detection. The variation of breast profile can cause differences in the contact pressure of each electrode which consequently causes variations in the electrode-skin impedance at different electrodes [68]. In addition, the heterogeneity of the skin layer

also contributes to the electrode-skin impedance [68]. Similar to most EIT systems, the ACT system suffered from bad contacts between the electrodes and the breast which were remedied by reconstructing the surface impedance of the individual electrodes to identify possible bad contacts [63]. This procedure has led to removing the unintended artifacts in some images [63].

C. Imaging Algorithms

Imaging algorithms for EIT usually assume quasi-static variations to simplify Maxwell's equations [69]–[73]. EIT imaging algorithms typically involve the solution of the *inverse problem* which is in general nonlinear, ill-posed and highly dependent on the electrode model, experimental errors, and noise [73]. There are two main classes of reconstruction algorithms: 1) linearized and 2) iterative methods [69]. In the first category, the inverse problem is simplified by assuming that the conductivities at different pixels in the breast do not significantly differ from a certain constant [69]. Examples of linearized methods are the back projection method, which is employed by the MEIK system, and the one-step Newton methods [69]. Iterative methods, such as the Gauss–Newton, typically require multiple solutions of the forward problem [72]. There are several ways to numerically solve the forward problem for the breast such as the finite-element method (FEM), the boundary-element method (BEM) or a hybrid FEM BEM method [71].

D. Clinical Trials

In a clinical study by Malich *et al.*, EIS was used to examine suspicious lesions detected by mammography and/or ultrasound [74]. In this study, 86 out of 103 malignant tumors and 91 out of 137 benign tumors were correctly diagnosed [74]. This corresponds to a sensitivity of 87.8% and 66.4%, respectively [74]. The EIS capability of distinguishing benign and malignant tumors is based on the differences in the impedance spectra of malignant and benign breast tissue reported in [75].

The clinical trials in [76] and [77] employed the T-Scan 2000ED which is an updated version of the FDA approved original T-Scan 2000 system. The clinical trials focused on the detection of tumors in women younger than 50 years old, which is the age group most prone to radiation concerns from X-ray mammography [77]. In addition, women in this age group typically have dense breasts where X-ray mammography is less sensitive in detecting tumors [76]. This clinical trial found that impedance values of breast tissue decrease with age and, therefore, higher thresholds have to be implemented in younger women than in older women [76]. In the age group of women younger than 40 years old, the sensitivity was 50% and the specificity was 90%. This specificity value was comparable to the specificity of mammography in younger women as reported in [77]. However, the authors emphasized that a larger group of patients needed to be tested to confirm the reported sensitivity and specificity values [76]. A follow up clinical study was performed in 2008 in [78] also for young women. The study concluded that if the T-Scan 2000ED system indicated that a tumor is present, then the patient was five times more likely to have breast cancer in comparison to a random individual.

V. Diffuse Optical Tomography (DOT)

A. Physical Parameter Sensed

Diffuse optical tomography (DOT) of breast cancer is defined as the use of light to image the optical properties of the breast interior. Compared to other breast cancer detection modalities, DOT uses significantly higher frequencies in the near infra-red (NIR) range from about 650 to 950 nm in wavelength [79]–[81]. The absorption coefficient of breast tissues in the near infrared region is presented in [82]–[85]. The 650 to 950-nm wavelength range represents a spectral window where the penetration of light through the biological tissue is maximal and, therefore, larger imaging depth can be achieved. Breast diameters ranging from 5–10 cm are the typical sizes imaged by DOT, while imaging larger breasts with DOT could pose a challenge [86], [87]. The maximum incident optical power was determined by the maximum permissible exposure (MPE) defined by standards such as the "Safety of laser products—Part 1: Equipment classification and requirements" standard [88]. For example, the University of Pennsylvania DOT system emits on average 600 μW per frequency from the tip of each optical fiber [89]. DOT typically exhibits a minimum detected tumor size of 5–10 mm [16].

In mammography, the incident x-ray photons travel through the breast in straight lines; however, in DOT the NIR photons experience multiple scattering as they propagate through the breast [80]. The mean path length is in the order of 1 mm in DOT, therefore, within a few millimeters the directions of the photons are random similar to diffusing particles [80]. In this frequency range, the propagation of light through biological tissue can be approximated with reasonable accuracy using the diffusion equation and hence the name diffuse optical tomography.

In DOT, the optical properties of the biological tissues, primarily the absorption and the scattering coefficients, are reconstructed at different locations in the breast. The absorption coefficient at each pixel arises from the summation of the absorption of the different of chromophores or dyes at each pixel [90]. Therefore, the concentration of each chromophore at each pixel can be reconstructed using the absorption coefficient [90]. The prime chromophores reconstructed from the absorption coefficient are oxy-hemoglobin, deoxy-hemoglobin, and water. Hemoglobin is the primary oxygen carrier in the blood. An elevated oxidized or deoxidized hemoglobin concentration, indicated in the absorption coefficient, implies an increase in blood vasculature associated with malignant tumor angiogenesis. From the concentrations of oxy-hemoglobin and deoxy-hemoglobin, the hemoglobin oxygen saturation can be calculated [79]–[81], [90]–[92]. Due to the elevated activity of malignant tumors, their demand for oxygen typically exceeds the available supply. Therefore, the presence of a region with reduced oxygen saturation indicates the presence of cancerous tissue. These quantities can shed light on functional properties such as the metabolic activity of the tissue, the permeability of the tissue, and the level of angiogenesis which can be used in breast cancer detection and diagnosis [81]. As for the scattering coefficient, it indicates the granularity of the tissue which is different in cancerous and healthy tissue [79]–[81], [90]–[92].

In a case study, the total hemoglobin concentration (oxy-hemoglobin+deoxy-hemoglobin), the water level and the oxygen saturation were measured in the breast of a patient with infiltrating ductal carcinoma [92]. The tumor region had a total hemoglobin concentration, a water level, and an oxygen saturation of 45 micromolar, 85% and 72%, respectively, whereas the background tissue showed values of 35 micromolar, 65% and 76%, respectively [92]. As for the scattering coefficient, the measured values in the tumor regions indicated higher granularity than the background regions [92].

B. Imaging Systems

In DOT, three measurement techniques were implemented: 1) time domain (TD) where the source excites the breast with an ultrashort time domain pulse; 2) frequency domain (FD) where the source emits a modulated signal to excite the breast and the phase and amplitude of the scattered signal are detected; and 3) continuous wave (CW) or steady state (SS) where only the amplitude of the scattered signals are detected [79]. FD allows imaging at larger depth but unlike CW it requires sources that can be modulated, which is difficult to achieve for a large bandwidth of frequencies. However, this requirement can be waived for CW imaging and therefore CW DOT systems can operate at larger bandwidths [93]. Typically, frequency domain DOT systems consist of two simultaneous components: 1) a CW imaging component operating over a broad band, and 2) an FD imaging component operating over few frequencies [93], [94].

Currently, there are several DOTs which have been tested in clinical trials [87], [89], [93]–[95]. The laser breast scanner (LBS) constructed at the University of California Irvine's Beckman Laser Institute employs a handheld probe that employs both FD and SS DOT [93], [94]. In the FD mode, seven RF modulated frequencies between 672 and 978 nm were employed, whereas in the SS mode a useful bandwidth of 650 to 1000 nm was employed. Another DOT system developed at Dartmouth College consists of 16 sources and 16 detectors arranged in a cylindrical array. The patient lies in the prone position with the breast hanging through the gap surrounded by the sources and detectors [87], [95]. The Dartmouth College DOT system employs FD imaging using RF modulated frequencies between 700–850 nm [87], [95]. A third system developed by the University of Pennsylvania adopted the FD and CW hybrid modality but with the sensor and detector arrays arranged on two parallel plates [89]. The breast is placed between these two parallel plates and compressed. A cylindrical array provides more coverage of the breast in comparison to the compressed parallel plate arrangement, but the compressed parallel plate arrangement is simpler and also provides more transmission depth and resolution [89]. The FD mode of the DOT system developed at the University of Pennsylvania employed four frequencies between 690 and 830 nm and involved an array of 45 sources [89]. A fourth system is the commercial system developed by Advanced Research Technologies (ART) [96]. The system consists of a single source and five detectors arranged to form an X-shape. The source and the detectors are moved concurrently to scan the breast. Unlike the other three DOT systems, the system developed by ART operates in the time domain [96]. The previous four systems were selected as the state of the art in DOT in [94].

The NIR light generated by laser sources is typically conveyed to the breast via optical fibers [94]. The end tip of the optical fiber is usually held in contact with the breast similar to the LBS system, the Dartmouth college system, and the University of Pennsylvania system [94]. In the University of Pennsylvania system the end tips of the optical fibers are integrated to one of the compressing planes [94]. In some systems, an antireflective surface is inserted between the end of the optical fiber and the breast to act as a compression plane [94]. As for the receivers, they can also consist of contacting optical fibers as in the Dartmouth college system or they can consist of a contactless camera as in the University of Pennsylvania system [94]. Therefore, in general, DOT is a contacting-based technique.

C. Imaging Algorithms

In parallel to the advances in DOT systems, there have been significant advances in the associated imaging algorithms [97]–[99]. Similar to other imaging modalities, DOT imaging algorithms typically involve the solution of both the *forward* and *inverse* problem [97]–[99]. The forward problem is the calculation of the scattered signals from the breast due to a certain incidence. The inverse problem is the retrieval of the breast tissue properties using the collected scattered signals. Solving the forward and inverse problem can be accomplished through analytical or statistical optimization techniques [97], [98]. Recent advances in DOT imaging involve using *a priori* information in the imaging algorithm. This *a priori* information could consist of the anatomical structure of the breast which could be obtained from traditional imaging modalities such as MRI or mammography. DOT would then use this anatomical structure to more accurately reconstruct the functionality of the region of interest. For example, the recent computational work by Jagannath *et al.* involved using the anatomical structure obtained from traditional imaging techniques to determine the finite element meshing in the three dimensional inverse problem of DOT [99]. This scheme enhanced the accuracy of the imaging of the optical properties of the biological tissue [99].

D. Clinical Trials

In a clinical study by Choe *et al.*, the DOT was used to reconstruct the optical parameters of 51 suspicious breast lesions [86]. The lesions were then classified using biopsies and 41 lesions were classified as malignant and ten were classified as benign [86]. In the study, the measured parameters were the relative total hemoglobin concentration (rTHC), relative blood oxygen saturation (rSTO2), relative deoxy-hemoglobin concentration (rHb), relative oxy-hemoglobin concentration (rHbO2), and relative scattering coefficient $r\mu_s'$. These parameters were termed relative since they were calculated by dividing the average values in the tumor region with the average values in the normal regions. The tumor regions were estimated using the MRI or the mammography and ultrasound. Additionally, the optical index (OI) was also calculated [86]. Four of these parameters were found to be statistically different in benign and

malignant tumors as: 1) relative total hemoglobin concentration; 2) relative oxy-hemoglobin concentration; 3) relative scattering coefficient; and 4) optical index [86]. The receiver operating characteristic (ROC) curve analysis was performed for each measured or calculated parameter and the four optimal parameters achieved at least 90% area under curve (AUC) corresponding to a sensitivity of 98% and a specificity of 90% [86]. Choe *et al.* proposed future improvements to his study by increasing the number of patients, especially those with benign lesions, and by more accurate reconstruction of the water content [86].

In a different clinical trial, by Poplack *et al.*, 18 malignant tumors and 40 benign lesions, in addition to 42 healthy patients were imaged using DOT. The performance of DOT was calculated for the subgroup with lesions 6 mm in diameter or larger. Using the reconstructed rTHC, an AUC of 88% was achieved in differentiating malignant from healthy patients and an AUC of 76% was achieved in differentiating malignant and benign lesions [16]. When the tumors less than 6 mm in diameter were considered, the AUC dropped [16].

Another important application of DOT is monitoring the response to chemotherapy [100], [101]. In a clinical trial conducted using the SoftScan platform, chemotherapy was monitored in ten patients with local advanced breast cancer [100], [101]. The optical parameters deoxyhemoglobin (Hb), oxyhemoglobin (HbO2), water percentage (%water), and scattering power (SP) were reconstructed [100], [101]. DOT was performed 3 days before and 1, 4, and 8 weeks after the start of the neoadjuvant chemotherapy [100], [101]. In the patients with a good response to the treatment, the average drop in Hb, HbO2, %water, and SP from the initial scan to the 4-week scan was 67.6%, 58.9%, 51.2%, and 52.6% $(\mathrm{SD} = 26.4)$, respectively. In contrast, the drop was only 17.7%, 18.0%, 15.4%, and 12.6%, respectively, for the cases which did not show a good response [100], [101]. These results are comparable to the 50% drop in Tissue Optical Index reported in a single patient with infiltrating ductal carcinoma at the end of the neoadjuvant chemotherapy period [102].

Contrast agents have also been investigated to increase the performance of DOT. Fluorescent contrast agents were tested in clinical trials [103] whereas light-absorbing contrast agents were tested in phantoms using a clinical system [104]. Fluorescent agents emit light at certain frequencies once excited by light in near infrared. However, the excitation light can be a source of noise in DOT [103]. On the other hand, the light-absorbing contrast agents, such as single-walled carbon nanotubes and black hole quencher-3, have the advantage of not needing light excitation. Both agent categories were tested for DOT with promising results [103], [104].

VI. Microwave Radiometry

A. Physical Parameter Sensed

Radiometry is defined as the passive detection of the radiation emitted by biological tissue at elevated temperatures [105]. Malignant breast tumors exhibit enhanced metabolism and elevated blood perfusion which increase their temperature, by 1°C to 3°C, in comparison to the surrounding breast tissue [105], [106]. Tissues at elevated temperature emit radiation at all frequencies peaking in the infrared region with less emission in the microwave region. However, due to the reduced transmission depth of infrared radiation in biological tissue (in the order of millimeters), in comparison to microwave radiation (in the order of centimeters), microwave radiometry had been proposed for breast cancer detection since the 1970s [105]. Microwave radiometry is a functional imaging modality since it detects the elevated microwave emission due to the high activity of the tumor. In microwave radiometry, the sensor is an antenna which detects the emitted radiation. This antenna can be placed directly on the breast or away from the breast, therefore, microwave radiometry can be a contacting or contactless technique [105]. However, in most cases the antenna is placed in direct contact with the breast to improve sensitivity and reduce the mismatch caused by the air layer between the antenna and the breast [106]–[108].

B. Imaging Systems

Breast compression is typically applied in mammography and other breast cancer detection modalities. This compression deforms the breast leading to changes in the distance between the tumor and the sensing antenna [108]. Iudicello *et al.* developed a coupled mechanical, thermal, and electromagnetic model to study the changes in the radiometric visibility of a tumor due to breast compression [108]. The model showed that the maximum detection depth of a 1 cm tumor in an uncompressed breast was $\approx$2.5 cm. If a 35% compression of the breast is applied the maximum detection depth increased to a value between 3 and 4.5 cm depending on the dielectric properties of the breast tissue [108].

A primary challenge in microwave radiometry of breast cancer is the low sensitivity sensor, or antenna, with respect to the small microwave signal emitted by the temperature-elevated tumor [105]. However, in a recent study antennas integrated directly with low noise amplifiers (LNA), termed active antennas, were tested for medical microwave radiometry [107]. At the operating frequency, the LNA provided a gain of 14.2 dB with a noise figure of 0.8 dB. The active antenna was found to significantly increase the detection of a hot object placed at a depth of 38 mm in an experimental phantom [107].

Due to the week nature of the signal in microwave radiometry, errors in the measurement can be attributed to external electromagnetic interference, such as wireless devices, and internal electromagnetic interference due to the radiometry device itself. External electromagnetic interference can be alleviated by shielding and careful design of the radiometer can reduce internal interference [107]. In addition, drift in the radiometer gains and parameters can lead to errors in the measurements which can be alleviated by a continuous recalibration of the radiometer using a Dicke switch demodulator [109].

C. Numerical Study

In a numerical study, which incorporated realistic heat generation by growing tumors, the visibility of breast tumors was estimated under the assumption of ideal antennas using the Pennes equation [106]. The result concluded that a 10-mm tumor can be detected if it is no more than 3 cm deep in the breast [106]. A smaller tumor, 6 mm in diameter, would require being less than 1 cm in depth to be detected [106]. In another numerical study,

the brightness temperatures of malignant tumors were numerically calculated using the method of moments [110]. The results showed that the brightness temperature of tumors exhibits a unique resonant behavior dependent only on the tumor properties and not its depth [110]. These resonances can provide future guidelines on the radiometer system parameters such as the optimum operating frequency [110].

D. Clinical Trials

In a clinical study, performed using the ONCOSCAN system, a probe was used to scan 20 positions distributed symmetrically among both breasts of 129 patients. The probe is placed at each location for 15 s before moving to the following location [111]. The study revealed a sensitivity of 90% and a specificity of 59% [111].

In another preliminary clinical trial that involved five breast cancer patients, the performance of two radiometers were compared [112]. The first radiometer operated in the 1.5–2 GHz frequency range whereas the second radiometer operated in the 2.75–3.25 GHz range [112]. In this clinical trial, four breast cancer patients had tumors at depth of 5–30 mm and were correctly detected using either one or two radiometers. However, the fifth patient had a tumor 30–40 mm deep which was not detected by either radiometer [112]. The results of the clinical trial also suggested that the first radiometer, operating at lower frequency, was more capable of detecting deeper tumors whereas the second radiometer, operating at higher frequency, was more capable of detecting smaller tumors (∼1 cm in diameter).

VII. Biopotential Detection

A. Physical Parameter Sensed

The biopotential detection technique depends on the passive detections of the biopotential signals generated by cancerous cells. Therefore, the biopotential detection modality is hypothesized to generate complimentary information to the nonpassive detection techniques. Biopotential detection of breast cancer has only been recently introduced and developed [113]–[119]. As cancerous cells divide they change their membrane potential by regulating their internal ion concentrations. These ion concentration regulations lead to imbalances in the concentrations of charged ions in the surrounding breast tissue which leads to biopotentials at the surface of the breast. To detect these biopotentials, a map of biopotential electrodes was placed on the breast with the suspicious lesion (Ipsilateral breast) and the other breast (Contralateral breast) as shown in Fig. 1 [119].

In the biopotential detection technique, silver/silver chloride electrodes filled with conductive cream were utilized and attached to the patient with adhesive collars [113]. Geometrical details of an electrode, optimized specifically for the biopotential detection of breast cancer, were presented by Faupel *et al.* in [120]. In addition, the chemical composition of the conjunctive conductive cream were also presented [120]. The sodium chloride naturally present on the skin of the patient can mask the biopotential signals generated by the tumor. Therefore, the conductive cream proposed by Faupel *et al.* had a certain concentration of chloride ion content, 6–15 grams per hundred of grams of cream, to compensate for this sodium chloride on the skin. The metallic parts of the electrode were optimized accordingly to avoid corrosion by this conductive cream [120].

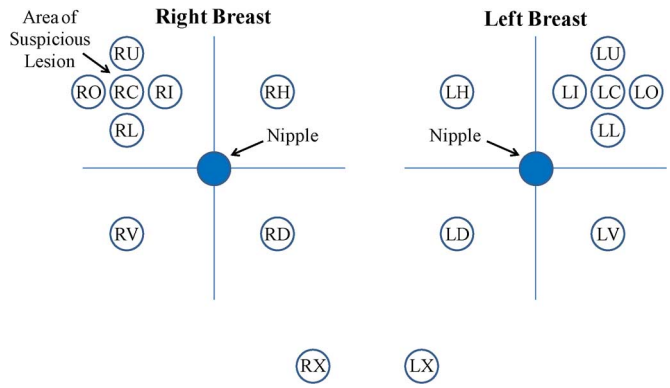

Fig. 1. Map of electrodes employed in biopotential detection of breast cancer [119].

B. Biopotential Systems

Currently, there is only one commercial biopotential system which is the CE certified Biofield Diagnostic System (BDS). The BDS system was developed originally by Biofield Corporation which is currently Mackay Life Sciences [121]. The BDS system uses the biopotentials measured on the surface of the breast in adjunction with the level of suspicion (LOS), calculated based on mammography or ultrasound results. Therefore, the BDS was CE certified to be used in conjunction with mammography or ultrasound [121]. The BDS system will then generate a Post-BDS LOS score to identify the risk of malignancy [122]. The BDS system, although CE certified, did not yet receive the FDA approval, which hinders its wide scale deployment.

C. Clinical Trials

The performance of the biopotential detection of breast cancer was tested in several clinical trials [115]–[119], [122]. The electrodes were typically arranged on the breasts as shown in Fig. 1 as follows. The electrodes on the right breast were marked with "R" and the electrodes on the left breast were marked with "L". In the configuration in Fig. 1, the suspicious legion was assumed to be in the right breast. The right breast was divided into four quadrants and in the quadrant with the tumor one electrode was placed on the breast surface directly above the center of the tumor "RC", one electrode was placed at the inner margin of the breast "RI", one electrode was placed at the outer margin of the breast "RO", one electrode was placed at the upper margin of the tumor "RU" and one electrode was placed at the lower margin of the tumor "RL" [119]. Three additional electrodes "RH", "RV", and "RD" were placed on the horizontal, vertical, and diagonal quadrants of the breast defined with respect to the quadrant with the tumor [119]. The electrode arrangement on the right breast was then mirrored on the contralateral breast [119]. Finally, two electrodes, RX and LX, were placed between the two breasts to act as the references for each breast [119]. In other measurement configurations, the reference electrodes were placed on the palms of the hands [117] or on the feet of the patients [114].

TABLE II
AVERAGE AND STANDARD DEVIATION OF BIOPOTENTIALS MEASURED FROM DIFFERENT LOCATIONS ON SURFACE OF BREAST DUE TO MALIGNANT AND BENIGN TUMORS [114]

Measurements Site	Cancer Cases (mV)	Benign Cases (mV)
Tumor (T)	21.4±12.4	17.1±10.3
Ipsilateral Control	17.4±12.8	16.9±8.9
T-IL	4.0±9.1	0.1±6.8
*T-*IL	-0.1±7.9	0.9±7.3
Contralateral Control	16.8±15.3	18.5±11.1
T-CL	4.5±9.4	-1.6±9.3

Table II summarizes the results achieved from a clinical experiment reported in [114] performed on 110 women, 29 with malignant tumors and 81 with benign tumors. In Table II, six measurements were shown [114]: tumor (T) which was the difference in biopotential between "RC" in Fig. 1 and the patient's feet, ipsilateral control which was the difference in biopotential between "RH" or "RV" in Fig. 1 and the patient's feet, T-IL which was the difference in biopotential between "RC" and "RH" or "RV", $^{*}\mathrm{T} - {}^{*}\mathrm{IL}$ which was the difference in biopotential between "LC" and "LH" or "LV", contralateral control which was the difference in biopotential between "LC" in Fig. 1 and the patient's feet and T-CL which was the difference in biopotential between "RC" and "LC" [114]. The results from Table II indicate that the tumor location is more electropositive in comparison to the locations on the ipsilateral breast away from the center of the tumor (T-IL). When the same potential difference was measured on the contralateral breast with no tumor $({}^{*}\mathrm{T} - {}^{*}\mathrm{IL})$ the potential difference had approximately a zero average as shown in Table II. In addition, when measuring the biopotential difference between the tumor location and the mirror location on the contralateral breast (T-CL) it was also found to be electropositive in average [114]. A noticeable feature in Table II was the large standard deviation in T-IL and T-CL.

In [116], the biopotential detection of breast cancer modality was tested in Japan in a population consisting of 49 patients with malignant breast tumors and 52 patients with benign breast tumors. A sensitivity of 90% and a specificity of 60% were achieved [116]. More importantly, the sensitivity was found to increase if only patients with lesions less than 2.5 cm in diameter were considered. The authors hypothesized that the reason for this rise in sensitivity for smaller tumors was the fact that they were still more actively growing in comparison to larger tumors [116]. A large clinical trial involving 661 patients in eight different centers in Europe was reported in [117]. An overall sensitivity of 90% and specificity of 55% was achieved and the best performance was achieved for palpable tumors.

In a recent clinical trial conducted in Singapore, the biopotential detection modality was used in conjunction with mammography and ultrasound [118]. The trial involved 103 patients, 19 with malignant tumors, 57 with benign tumors and 27 healthy patients [118]. The trial showed that combining the biopotential modality with mammography and/or ultrasound yielded a sensitivity of 100% and a specificity of 96% [118]. The authors recommended future testing of the modality with a larger population to confirm the previous results but the previous preliminary results indicate the merit of the biopotential detection of breast cancer.

In another clinical study, Vinitha Sree *et al.* investigated increasing the accuracy of the biopotential detection of breast cancer using the BDS system by applying data mining techniques on the following features: 1) demographic details of the patient; 2) the Post-BDS LOS score; and 3) raw recorded biopotentials [122]. In the first step, filter and wrapper methods were implemented to identify a reduced subset of the eight features that maximize sensitivity, specificity and accuracy [122]. Classifiers such as statistical inference techniques and artificial neural networks were then trained by a portion of the measurements and tested with the remaining measurements. The wrapper feature subset combined with a linear discriminant analysis (LDA) classifier yielded a sensitivity of 92.7%, a specificity of 98.4%, and an accuracy of 97% compared to a sensitivity of 89.6%, a specificity of 54.6% and an accuracy of 63.1% obtained using Post-BDS LOS alone [122]. More importantly, the wrapper feature subset did not include the Post-BDS LOS dependent on the mammography and ultrasound which shows that the biopotential detection technique can be used as an independent technique [122].

The biopotentials recorded in the previous clinical trials were in the millivolt range. Specifically, in the clinical study conducted by Fukuda *et al.*, the average values of T-IL were reported to be $\approx$12 mV for malignant tumors and $\approx$9.5 mV for benign tumors whereas the average values of T-CL were $\approx$4.2 mV for malignant tumors and $\approx$3.4 mV for benign tumors [116]. In the clinical study of Vinitha Sree *et al.*, the average values of T-IL were reported to be 5.2 mV for malignant tumors and 2.18 mV for benign tumors [122].

The development of more sensitive sensors and more accurate data mining algorithms is anticipated to significantly increase the adoption of the biopotential detection technique. Moreover, the mechanism by which tumors generate biopotential signals is not fully understood. Understanding this mechanism could provide possible explanations for the past clinical recordings of the biopotentials and could help assess the feasibility of this technology. Of particular interest is why the location on the breast skin above the tumor was in general more positive in biopotential and why the biopotential recordings had a large standard deviation as shown in Table II obtained from [114]. Also, the current performance of the biopotential detection technique is more accurate for palpable tumors than for non-palpable tumors [117]. This difference in performance can be attributed to the simplicity of placing the electrodes directly on top of a palpable lesion, whereas it is more challenging to figure out the location of a lesion based on mammography or ultrasound results [117]. Therefore, a persistent need demonstrated in the literature is to develop improved

sensors and mapping positions based on better understanding of the electrophysiological activities of growing tumors as discussed in [117] and [119].

D. Biopotential Signal Modeling

In order to address the previous challenges, a 2-D model was developed to calculate the electric current densities and the biopotentials generated from single and multiple breast cancer cells at different cell division stages [123]–[129]. Three cell division stages were considered: depolarization which occurs at the beginning of the Gap 1 (G1) stage; hyperpolarization which occurs between the G1 and Synthesis (S) stage; and quiescence where the cell neither depolarizes nor hyperpolarizes [125]–[129]. The goal of these works was to understand the electrophysiology of the breast cancer cell line termed Michigan Cancer Foundation-7 (MCF-7) [123]–[129]. The developed model was based on the semiconductor diffusion-drift analysis. For a single MCF-7 cell, it was concluded that the shorter the duration of the G1/S transition, and the higher the diffusivity and mobility at the cell boundary, the higher the magnitude of the generated electric signals [123], [124].

The model was extended to include multiple MCF-7 cells [125], [126]. Nonuniform finite-difference discretization was implemented to accommodate the contrast in size between the intercellular spacing and the cell dimension. The results showed that the biopotentials increase proportionally with the number of cells, especially when all cells were in the hyperpolarization stage [125], [126].

In order to increase the number of cells, the diffusion-drift algorithm was parallelized using the message passing interface (MPI) technique [127]–[129]. The computational bottleneck of the model involved the solutions of systems of equations, based on the Nernst-Plank, the Poisson, and the Continuity equations, to calculate the biopotentials and the ion concentrations. The Portable, Extensible Toolkit for Scientific Computation library was adopted for the solution of these equations [127]–[129]. The increase in speed from the parallelization allowed the simulation of significantly larger tumors [127]–[129].

As known, early stage tumor growth cancerous cells are prone to forces and interactions which generate highly complex tumor shapes. The generated electric signals of the most common tumor shape patterns, i.e. Papillary, Compact, and Comedo, were investigated [127]–[129]. The highest biopotential signal was observed from the compact tumor whereas the lowest biopotential signal was observed from the papillary pattern. Interestingly, the spatial distribution of the biopotential signals showed a shift in the maximum biopotential amplitude away from the top of the tumor. This shift indicated that the conventional sensor arrangement shown in Fig. 1, where a sensor was placed directly above the center of the tumor, might not be able to detect the maximum generated biopotentials in some cases. In addition, large temporal variations in the generated biopotentials were observed for different tumor shapes and cell distributions among the different cell division stages which could partially explain the large standard deviations seen in Table II. These observations can have important clinical implications when using the biopotential signals for breast cancer detection [127]–[129].

VIII. Biomagnetic Detection

In preliminary studies shown in [130]–[132], elevated magnetic fields were detected from malignant breast tumors in comparison to benign tumors. In [130], the biomagnetic fields from 11 patients with invasive breast carcinoma and ten with benign breast tumors were recorded. It was found that invasive breast carcinoma produced magnetic fields with higher magnitude and more fluctuations than benign tumors. On average, malignant tumors generated 754 $\mathrm{fT}/\sqrt{\mathrm{Hz}}$, whereas benign tumors generated 274 $\mathrm{fT}/\sqrt{\mathrm{Hz}}$ in the 2–7 Hz frequency range [131]. By employing nonlinear chaotic analysis the classification of malignant and benign tumors was achieved.

The results presented in [130]–[132] were highly preliminary in terms of the number of patients, the simplicity of the superconducting quantum interference device (SQUID) system used and the negligence of the other biomagnetic signals generated from the human body mentioned in [133]. The detection of the biomagnetic fields generated from excitable organs such as the brain has emerged as an important diagnostic modality which is termed magnetoencephalography (MEG). Recent developments in MEG include the development of whole head MEG system with few hundred SQUID sensors [133]. Similarly, the development of SQUID systems with a large number of detectors arranged to conform to the shape of the breasts is anticipated to increase the accuracy of the biomagnetic detection of breast cancer.

IX. Magnetic Resonance Imaging

A. Physical Quantity Sensed

Although the MRI is based on an electromagnetic phenomenon, it has different features. The MRI has emerged as a high resolution breast cancer detection method. In most medical imaging techniques, the limit on the resolution is set by the frequency or wavelength of the utilized radiation; however, in MRI two radiations are exerted to interact together which breaks the limit on resolution enforced by the wavelength criteria [134]. In MRI, the first radiation induces local interactions whereas the second radiation limits this local interaction into a certain region allowing imaging of different regions to be accomplished [134]. More specifically, in MRI a static magnetic field is exerted which aligns the magnetic moment of the hydrogen nuclei or protons composing the human body [135]. A radiofrequency (RF) pulse is then exerted at a certain frequency which is absorbed by the aligned hydrogen nuclei. The RF pulse has to be set at a certain frequency determined by the magnitude of the incident static magnetic field. The protons will then absorb this RF pulse causing a change in the direction of their magnetic moment. The protons will then relax to their stable state emitting RF pulses in the process.

Different tissues relax at different measurable rates which is the basis of identifying different tissue. In order to image different regions in the human body, gradients in the magnetic field are exerted. These gradients cause variations in the frequencies that the RF pulses emit as they get back to their stable state. Therefore, by measuring the frequency of the received RF pulses, the position they are coming from can be determined [135].

MRI for breast cancer has been proposed since the late 1970s but until the 1980s it did not show sufficient benefit [136]. However, the use of gadolinium as a contrast agent in MRI significantly enhanced breast cancer detection [136]. In almost all studies, MRI has exhibited high sensitivity and it often detected small tumors missed by mammography and ultrasound [136], [137]. MRI showed particular advantage in dense breasts where mammography typically fails to detect tumors. However, the elevated sensitivity of MRI came at the expense of modest specificity [136], [137].

Even though mammography is the golden standard for breast cancer screening and detection, MRI has been dominant in several scenarios such as: 1) high risk screening; 2) preoperative breast cancer staging; 3) evaluation for breast cancer recurrence; 4) localization of the primary tumor when lymph node metastases is detected; and 5) evaluation of breast cancer after neoadjuvant chemotherapy. MRI has been proposed for the screening of young women where mammography can cause fertility issues or can be inaccurate due to the elevated density of the breast [137]. Also, MRI has been utilized in patients with increased risk of breast cancer due to genetic reasons or due to the prior detection of tumors.

B. Imaging Systems

There are two prominent kinds of medical imaging techniques: 1) anatomical and 2) functional [138]. In conventional MRI, gadolinium is administered as a contrast agent to clarify the differences in anatomy between cancerous and healthy tissues. This is termed dynamic contrast-enhanced (DCE)-MRI [138]–[140]. As the tumor gets smaller, it becomes more difficult to detect using only its anatomical appearance [138]. In functional imaging, physiological changes in tumors are utilized to distinguish them from healthy regions [138]. A relatively new functional MRI modality, termed diffusion weighted imaging (DWI) has recently shown promise in breast cancer detection [138]–[140]. DWI MRI does not require a contrast agent and it is based on the fact that tumor tissue has increased cellular density which restricts the flow of water. DWI MRI probes the flow of water and, therefore, tumor tissue appears to have a lower apparent diffusion coefficient (ADC) than normal tissue allowing for their detection [138]–[140]. In a preliminary study, Iima *et al.* measured the ADC of the tumor regions in 22 patients with ductal carcinoma *in situ* (DCIS), which is breast cancer where the cells are still confined within the ducts [139]. Normal, low grade, intermediate grade, and high grade DCIS yielded ADC values of 1.42×10^{-3} mm^2/s, 1.23 mm^2/s, 1.19 mm^2/s, and 2.06 mm^2/s, respectively, indicating to the discriminatory value of DWI MRI [139]. This was corroborated by another preliminary study which showed that 91% sensitivity in the detection of DCIS was achieved by using a threshold in ADC [140].

C. Clinical Studies

In a study in The Netherlands that involved 1909 patients, with at least 15% risk of breast cancer due to family or genetic factors, MRI exhibited a sensitivity of 79.5%, compared to a sensitivity of 17.9% and 33.3%, achieved using clinical examination and mammography [141]. In addition, MRI achieved a specificity of 89.8% compared to a specificity of 98.1% and 95.0% achieved using clinical examination and mammography [141]. In a similar study in Germany involving 529 high risk patients, MRI provided a sensitivity of 91% compared to a sensitivity of 33%, 40%, and 49% obtained using mammography, ultrasound, and a combination of mammography and ultrasound, respectively [142]. Therefore, in conclusion, MRI is more sensitive in detecting breast cancer in high risk patients [141], [142].

Another application of MRI is the evaluations of the extent of the tumor prior to treatment. In a study of 59 patients, Esserman *et al.* showed that MRI was accurate in assessing the extent of the tumor in 98% of the cases compared to 55% of the cases using mammography [143]. Focusing only on invasive lobular carcinoma (ILC), MRI was sensitive in detecting the extent of the tumor in 85% of the cases compared to 31% of the cases using mammography [137]. As for DCIS the sensitivity of MRI ranged from 40% to 100% in accurately assessing the extent of the tumor [137]. However, in a recent study by Menell *et al.*, MRI exhibited a higher sensitivity, 88%, compared to a sensitivity of 27% in mammography [144]. The authors explained this relatively higher sensitivity by clarifying that each pixel in MRI has an intensity proportional to the volume average of its contents [144]. In DCIS, in particular, the cancerous tissues are closely interleaved with healthy tissue. Therefore, if the pixel size in MRI is large, the cancerous regions will appear to be less bright, as the signal is weakened by the healthy tissue. In the study of Menell *et al.*, higher resolution was employed and therefore DCIS tumors were better resolved [144]. The study of Menell *et al.* was further corroborated in a study by Kuhl *et al.* in 2007 where MRI detected 87 out of 89 high grade DCIS compared to 46 detected by mammography [145].

In a similar manner, MRI was found to be more accurate than ultrasound, mammography, and clinical examination in detecting recurring tumors. However, some false positives were detected when the imaging was performed within a short period of the treatment. Another scenario where MRI typically excels is the localization of the primary tumor when metastases are detected in the lymph nodes. If the primary tumor is not detected, the drastic mastectomy of the whole breast will be typically employed [137]. MRI is typically more accurate in detecting the primary tumor even in the challenging cases missed by other imaging modalities [137].

The treatment of locally advanced breast cancer usually involves the administration of chemotherapy to shrink the tumor before surgical intervention. MRI has been utilized in assessing the effectiveness of chemotherapy before removal of the tumor with sensitivities as high as 97% [137]. However, a notable observation is the gradual reduction in the enhancement in tumor regions in MRI images as more chemotherapy rounds are administered which might reduce the sensitivity [137]. However, other researchers used this gradual decrease in enhancement of the tumor regions in MRI images as an indication to the effectiveness of the chemotherapy. In a study by Tsuboi *et al.* involving 31 patients, 15 tumors exhibited reduction in the enhancement of the tumor regions and 9 out of those 15 exhibited negative surgical margins [146]. In the 16 tumors that exhibited no decrease in the enhancement in the tumor regions in the

MRI images, 12 had positive surgical margins indicating that chemotherapy was not effective [146].

In summary, MRI has several advantages such as a high sensitivity, no ionizing radiation, and the ability to image radiographically dense breast [147]. However, the prime limitation of MRI is the high cost of imaging [147], [148]. A bilateral breast MRI costs around $1025 dollars whereas a mammography costs $85 [148]. A reduction in this cost will significantly increase the use of MRI in breast cancer screening. Other limitations include the large variety in the reported specificity values, the large processing time, and the necessity of the expensive intravenous contrast agent, gadolinium, in dynamic contrast-enhanced (DCE)-MRI [147].

X. Conclusion

Each section in this paper provided an up-to-date status of research in seven electromagnetic modalities for breast cancer detection. It is evident that EM techniques show high potential to improve the detection of breast cancer. On the other hand, EM techniques still face major challenges and limitations that need to be overcome before they can be introduced into wide scale utilizations in clinics. Integrating more than one EM technique has shown a potential to resolve some of these limitations.

References

[1] R. Siegel, E. Ward, O. Brawley, and A. Jemal, "Cancer statistics, 2011: The impact of eliminating socioeconomic and racial disparities on premature cancer deaths," *CA Cancer J. Clin.*, vol. 61, no. 4, pp. 212–236, 2011.

[2] L. Tabár and P. Dean, "A new era in the diagnosis and treatment of breast cancer," *J. Breast*, vol. 16, pp. S2–S4, 2010.

[3] L. Tabar, C. Fagerberg, A. Gad, and L. Baldetorp *et al.*, "Reduction in mortality from breast cancer after mass screening with mammography: Randomised trial from the Breast Cancer Screening Working Group of the Swedish National Board of Health and Welfare," *Lancet*, vol. 325, no. 8433, pp. 829–832, Apr. 1985.

[4] B. Hellquist, S. Duffy, S. Abdsaleh, L. Björneld, P. Bordás, L. Tabár, B. Viták, S. Zackrisson, L. Nyström, and H. Jonsson, "Effectiveness of population-based service screening with mammography for women ages 40 to 49 years: Evaluation of the Swedish mammography Screening in Young Women (SCRY) cohort," *Cancer*, vol. 117, no. 4, pp. 714–722, 2011.

[5] U.S. Preventive Services Task Force, "Screening for breast cancer: U.S. preventive services task force recommendation statement," *Ann. Internal Medicine*, vol. 151, no. 10, pp. 716–726, 2009.

[6] M. Kalager, M. Zelen, F. Langmark, and H. Adami, "Effect of screening mammography on breast-cancer mortality in Norway," *New Engl. J. Med.*, vol. 363, no. 13, pp. 1203–1210, Sep. 2010.

[7] E. Fear, S. Hagness, P. M. Okoniewski, and M. Stuchly, "Enhancing breast tumor detection with near-field imaging," *IEEE Microw. Mag.*, vol. 3, no. 1, pp. 48–56, Mar. 2002.

[8] E. Ng, S. Sree, K. Ng, and G. Kaw, "The use of tissue electrical characteristics for breast cancer detection: A perspective review," *Technol. Cancer Res. Treatment*, vol. 7, no. 4, pp. 295–308, 2008.

[9] M. El-Shenawee, "Electromagnetic imaging for breast cancer research," in *Proc. 2011 IEEE Radio Wireless Symp.*, Phoenix, AZ, Jan. 16–19, 2011.

[10] P. Huynh, A. Jarolimek, and S. Daye, "The false-negative mammogram," *RadioGraphics*, vol. 18, pp. 1137–1154, 1998.

[11] A. Berrington de González and S. Darby, "Risk of cancer from diagnostic X-rays: Estimates for the U.K. and 14 other countries," *Lancet*, vol. 363, no. 9406, pp. 345–351, Jan. 2004.

[12] C. Ronckers, C. Erdmann, and C. Land, "Radiation and breast cancer: A review of current evidence," *Breast Cancer Res.*, vol. 7, no. 1, pp. 21–32, Nov. 2004.

[13] D. Ikeda, D. Baker, and B. Daniel, "Magnetic resonance imaging of breast cancer: Clinical indications and breast MRI reporting system," *J. Magnet. Resonance Imag.*, vol. 12, pp. 975–983, 2000.

[14] S. Orel and M. Schnall, "MR imaging of the breast for the detection, diagnosis, and staging of breast cancer," *Radiology*, vol. 220, no. 1, pp. 13–30, 2001.

[15] W. Berg, L. Gutierrez, M. NessAiver, W. Carter, M. Bhargavan, R. Lewis, and O. Ioffe, "Diagnostic accuracy of mammography, clinical examination, U.S., and MR imaging in preoperative assessment of breast cancer," *Radiology*, vol. 233, pp. 830–849, Dec. 2004.

[16] S. Poplack, T. Tosteson, W. Wells, B. Pogue, P. Meaney, A. Hartov, C. Kogel, S. Soho, J. Gibson, and K. Paulsen, "Electromagnetic breast imaging: Results of a pilot study in women with abnormal mammograms," *Radiology*, vol. 243, pp. 350–359, 2007.

[17] P. Meaney, M. Fanning, D. Li, S. Poplack, and K. Paulsen, "A clinical prototype for active microwave imaging of the breast," *IEEE Trans. Microw. Theory Techniques*, vol. 48, no. 11, pp. 1841–1853, Nov. 2000.

[18] M. Klemm, I. Craddock, J. Leendertz, A. Preece, and R. Benjamin, "Radar-based breast cancer detection using a hemispherical antenna array—Experimental results," *IEEE Trans. Antennas Propagat.*, vol. 57, no. 6, pp. 1692–1704, Jun. 2009.

[19] C. Yu, M. Yuan, J. Stang, E. Bresslour, R. George, G. Ybarra, W. Joines, and Q. Liu, "Active microwave imaging II: 3-D system prototype and image reconstruction from experimental data," *IEEE Trans. Microw. Theory Tech.*, vol. 56, no. 4, pp. 991–1000, Apr. 2008.

[20] W. Huang and A. Kishk, "Compact dielectric resonator antenna for microwave breast cancer detection," *IET Microwaves, Antennas Propagat.*, vol. 3, no. 4, pp. 638–644, Jun. 2009.

[21] M. Al-Joumayly, S. Aguilar, N. Behdad, and S. Hagness, "Dual-band miniaturized patch antennas for microwave breast imaging," *IEEE Antennas Wireless Propagat. Lett.*, vol. 9, pp. 268–271, 2010.

[22] D. Gibbins, M. Klemm, I. Craddock, J. Leendertz, A. Preece, and R. Benjamin, "A comparison of a wide-slot and a stacked patch antenna for the purpose of breast cancer detection," *IEEE Trans. Antennas Propagat.*, vol. 58, no. 3, pp. 665–674, Mar. 2010.

[23] J. Bourqui, M. Okoniewski, and E. Fear, "Balanced antipodal Vivaldi antenna with dielectric director for near-field microwave imaging," *IEEE Trans. Antennas Propagat.*, vol. 58, no. 7, pp. 2318–2326, Jul. 2010.

[24] X. Li, S. Hagness, M. Choi, and D. van der Weide, "Numerical and experimental investigation of an ultrawideband ridged pyramidal-horn antenna with curved launching plane for pulse radiation," *IEEE Antennas Wireless Propagat. Lett.*, vol. 2, pp. 259–262, 2003.

[25] R. Amineh, A. Trehan, and N. Nikolova, "TEM horn antenna for ultra-wide band microwave breast imaging," *Progress Electromagnet. Res. B*, vol. 13, pp. 59–74, 2009.

[26] D. Hutchings and M. El-Shenawee, "Fabrication of broadband MEMS antennas and application to target detection," in *Proc. IEEE Int. Symp. Antennas Propagation USNC/URSI Nat. Radio Sci. Meeting*, Toronto, Canada, Jul. 11–17, 2010.

[27] D. Woten, M. El-Shenawee, and S. Tung, "Planar broadband dual-linearly polarized MEMS steerable antenna," in *Proc. IEEE Int. Symp. Antennas Propagation/URSI Nat. Radio Sci. Meeting*, Charleston, SC, Jun. 1–5, 2009.

[28] D. Woten and M. El-Shenawee, "Broadband dual linear polarized antenna for statistical detection of breast cancer," *IEEE Trans. Antennas Propagat.*, vol. 56, no. 11, pp. 3576–3580, Nov. 2008.

[29] D. Winters, J. Shea, E. Madsen, G. Frank, B. Van Veen, and S. Hagness, "Estimating the breast surface using UWB microwave monostatic backscatter measurements," *IEEE Trans. Biomed. Eng.*, vol. 55, no. 1, pp. 247–256, Jan. 2008.

[30] T. Williams, J. Sill, and E. Fear, "Breast surface estimation for radar-based breast imaging systems," *IEEE Trans. Biomed. Eng.*, vol. 55, no. 6, pp. 1678–1686, Jun. 2008.

[31] T. Williams, E. Fear, and D. Westwick, "Tissue sensing adaptive radar for breast cancer detection—Investigations of an improved skin-sensing method," *IEEE Trans. Microw. Theory Techn.*, vol. 54, no. 4, pp. 1308–1314, Jun. 2006.

[32] A. Abubakar, P. van den Berg, and J. Mallorqui, "Imaging of biological data using a multiplicative regularized contrast source inversion method," *IEEE Trans. Microw. Theory Techn.*, vol. 50, no. 7, pp. 1761–1771, Jul. 2002.

[33] A. Bulyshev, A. Souvorov, S. Semenov, V. Posukh, and Y. Sizov, "Three-dimensional vector microwave tomography: Theory and computational experiments," *Inv. Probl.*, vol. 20, pp. 1239–1259, 2004.

[34] Q. Fang, P. S. Geimer, A. Streltsov, and K. Paulsen, "Microwave image reconstruction from 3-D field coupled to 2-D parameter estimation," *IEEE Trans. Med. Imag.*, vol. 23, no. 4, pp. 475–484, Apr. 2004.

[35] Z. Zhang and Q. Liu, "Three-dimensional nonlinear image reconstruction for microwave biomedical imaging," *IEEE Trans. Biomed. Eng.*, vol. 51, no. 3, pp. 544–548, Mar. 2004.

[36] E. Fear and M. Stuchly, "Microwave detection of breast cancer," *IEEE Trans. Microw. Theory Tech.*, vol. 48, no. 11, pp. 1854–1863, Nov. 2000.

[37] X. Li and S. Hagness, "A confocal microwave imaging algorithm for breast cancer detection," *IEEE Microw. Wireless Compon. Lett.*, vol. 11, no. 3, pp. 130–132, Mar. 2001.

[38] E. Fear, X. Li, S. Hagness, and M. Stuchly, "Confocal microwave imaging for breast cancer detection: Localization of tumors in three dimensions," *IEEE Trans. Biomed. Eng.*, vol. 49, no. 8, pp. 812–822, Aug. 2002.

[39] E. Fear, J. Sill, and M. Stuchly, "Experimental feasibility study of confocal microwave imaging for breast tumor detection," *IEEE Trans. Microw. Theory Techn.*, vol. 51, no. 3, pp. 887–892, Mar. 2003.

[40] E. Bond, S. Hagness, and B. Van Veen, "Microwave imaging via space-time beamforming for early detection of breast cancer," *IEEE Trans. Antennas Propagat.*, vol. 51, no. 8, pp. 1690–1705, Aug. 2003.

[41] X. Li, S. Davis, S. Hagness, D. van der Weide, and B. Van Veen, "Microwave imaging via space-time beamforming: Experimental investigation of tumor detection in multilayer breast phantoms," *IEEE Trans. Microw. Theory Techn.*, vol. 52, no. 8, pp. 1856–1865, Aug. 2004.

[42] S. Davis, H. Tandradinata, S. Hagness, and B. Van Veen, "Ultrawideband microwave breast cancer detection: A detection-theoretic approach using the generalized likelihood ratio test," *IEEE Trans. Biomed. Eng.*, vol. 52, no. 7, pp. 1237–1250, Jul. 2005.

[43] P. Kosmas and C. Rappaport, "Time reversal with the FDTD method for microwave breast cancer detection," *IEEE Trans. Microw. Theory Techn.*, vol. 53, no. 7, pp. 2317–2323, Jul. 2005.

[44] M. El-Shenawee and E. Miller, "Spherical harmonics microwave algorithm for shape and location reconstruction of breast cancer tumor," *IEEE Trans. Medical Imaging*, vol. 25, no. 10, pp. 1258–1271, Oct. 2006.

[45] M. El-Shenawee, O. Dorn, and M. Moscoso, "Adjoint-field technique for shape reconstruction of 3-D penetrable object immersed in lossy medium," *IEEE Trans. Antennas Propagat.*, vol. 57, no. 2, pp. 520–534, Feb. 2009.

[46] M. El-Shenawee, "Resonant spectra of malignant breast cancer tumors using the three-dimensional electromagnetic fast multipole model," *IEEE Trans. Biomed. Eng.*, vol. 51, no. 1, pp. 35–44, Jan. 2004.

[47] P. Meaney, M. Fanning, T. Raynolds, C. Fox, Q. Fang, C. Kogel, S. Poplack, and K. Paulsen, "Initial clinical experience with microwave breast imaging in women with normal mammography," *Acad. Radiol.*, vol. 14, pp. 207–218, 2007.

[48] M. Klemm, I. Craddock, J. Leendertz, A. Preece, and R. Benjamin, "Experimental and clinical results of breast cancer detection using UWB microwave rada," in *Proc. IEEE Int. Symp. Antennas Propagation USNC/URSI Nat. Radio Sci. Meeting*, San Diego, CA, Jul. 5–12, 2008.

[49] M. Lazebnik, L. McCartney, D. Popovic, C. Watkins, M. Lindstrom, J. Harter, S. Sewall, A. Magliocco, J. Booske, M. Okoniewski, and S. Hagness, "A large-scale study of the ultrawideband microwave dielectric properties of normal breast tissue obtained from reduction surgeries," *Physics Medicine Biol.*, vol. 52, pp. 2637–2656, Apr. 2007.

[50] M. Lazebnik, D. Popovic, L. McCartney, C. Watkins, M. Lindstrom, J. Harter, S. Sewall, T. Ogilvie, A. Magliocco, T. Breslin, W. Temple, D. Mew, J. Booske, M. Okoniewski, and S. Hagness, "A large-scale study of the ultrawideband microwave dielectric properties of normal, benign, and malignant breast tissues obtained from cancer surgeries," *Phys. Medicine Biol.*, vol. 52, pp. 6093–6115, 2007.

[51] J. Shea, P. Kosmas, S. Hagness, and B. Van Veen, "Three-dimensional microwave imaging of realistic numerical breast phantoms via a multiple-frequency inverse scattering technique," *Med. Phys.*, vol. 37, no. 8, pp. 4210–4226, Aug. 2010.

[52] R. Halter, T. Zhou, P. A. Hartov, R. Barth, Jr., K. Rosenkranz, W. Wells, C. Kogel, A. Borsic, E. Rizzo, and K. Paulsen, "The correlation of *in vivo* and *ex vivo* tissue dielectric properties to validate electromagnetic breast imaging: Initial clinical experience," *Physiolog. Measure.*, vol. 30, no. 6, pp. S121–S136, Jun. 2009.

[53] M. Zhao, J. Shea, S. Hagness, D. van der Weide, B. Van Veen, and T. Varghese, "Numerical study of microwave scattering in breast tissue via coupled dielectric and elastic contrasts," *IEEE Antennas Wireless Propagat. Lett.*, vol. 7, pp. 247–250, 2008.

[54] B. Xie, J. Weaver, P. Meaney, and K. Paulsen, "Magnetic resonance microwave absorption imaging: Feasibility of signal detection," *Med. Phys.*, vol. 36, no. 11, pp. 5190–5197, Nov. 2009.

[55] A. Mashal, J. Booske, and S. Hagness, "Toward contrast-enhanced microwave-induced thermoacoustic imaging of breast cancer: An experimental study of the effects of microbubbles on simple thermoacoustic targets," *Phys. Medicine Biol.*, vol. 54, pp. 641–650, 2009.

[56] A. Mashal, B. Sitharaman, X. Li, P. Avti, A. Sahakian, J. Booske, and S. Hagness, "Toward carbon-nanotube-based theranostic agents for microwave detection and treatment of breast cancer: Enhanced dielectric and heating response of tissue-mimicking materials," *IEEE Trans. Biomed. Eng.*, vol. 57, no. 8, pp. 1831–1834, Aug. 2010.

[57] J. Shea, P. Kosmas, S. Hagness, and B. Van Veen, "Contrast-enhanced microwave imaging of breast tumors: A computational study using 3-D realistic numerical phantoms," *Inverse Problems*, vol. 26, p. 074009, 2010.

[58] Y. Chen, I. Craddock, and P. Kosmas, "Feasibility study of lesion classification via contrast-agent-aided UWB breast imaging," *IEEE Trans. Biomed. Eng.*, vol. 57, no. 5, pp. 1003–1007, May 2010.

[59] M. Blomley, J. Cooke, E. Unger, M. Monaghan, and D. Cosgrove, "Microbubble contrast agents: A new era in ultrasound," *Brit. Med. J.*, vol. 322, no. 7296, pp. 1222–1225, 2001.

[60] E. Stride and N. Saffari, "Microbubble ultrasound contrast agents: A review," *Proc. Inst. Mech. Eng.*, vol. 217, no. 6, pp. 429–447, 2003.

[61] M. Uo, T. Akasaka, F. Watari, Y. Sato, and K. Tohji, "Toxicity evaluations of various carbon nanomaterials," *Dental Mater. J.*, vol. 30, no. 3, pp. 245–263, 2011.

[62] T. Kerner, K. Paulsen, A. Hartov, S. Soho, and S. Poplack, "Electrical impedance spectroscopy of the breast: Clinical imaging results in 26 subjects," *IEEE Trans. Med. Imag.*, vol. 21, no. 6, pp. 638–645, Jun. 2002.

[63] G. Boverman, D. Isaacson, G. Saulnier, and J. Newell, "Methods for compensating for variable electrode contact in EIT," *IEEE Trans. Biomed. Eng.*, vol. 56, no. 12, pp. 2762–2772, Dec. 2009.

[64] G. Boverman, T. Kao, R. Kulkarni, B. Kim, D. Isaacson, G. Saulnier, and J. Newell, "Robust linearized image reconstruction for multifrequency EIT of the breast," *IEEE Trans. Med. Imag.*, vol. 27, no. 10, pp. 1439–1448, Oct. 2008.

[65] S. Vinitha Sree, E. Ng, R. Acharya-U, and W. Tan, "Breast imaging systems: A review and comparative study," *J. Mechanics Medicine Biol.*, vol. 10, no. 1, pp. 5–34, 2010.

[66] V. Cherepenin, A. Karpov, A. Korjenevsky, V. Kornienko, A. Mazaletskaya, D. Mazourov, and J. Meister, "A 3-D electrical impedance tomography (EIT) system for breast cancer detection," *Physiol. Meas.*, vol. 22, pp. 9–18, 2001.

[67] V. Cherepenin, A. Karpov, A. Korjenevsky, V. Kornienko, Y. Kultiasov, M. Ochapkin, O. Trochanova, and J. Meister, "Three-dimensional EIT imaging of breast tissues: System design and clinical testing," *IEEE Trans. Med. Imag.*, vol. 21, no. 6, pp. 662–667, Jun. 2002.

[68] E. Demidenko, A. Borsic, Y. Wan, R. Halter, and A. Hartov, "Statistical estimation of EIT electrode contact impedance using magic Toeplitz matrix," *IEEE Trans. Biomed. Eng.*, vol. 58, no. 8, pp. 2194–2201, Aug. 2011.

[69] M. Cheneyy, D. Isaacsony, and J. Newell, "Electrical impedance tomography," *SIAM Rev.*, vol. 41, no. 1, pp. 85–101, 1999.

[70] R. Bayford, "Bioimpedance tomography (electrical impedance tomography)," *Annu. Rev. Biomed. Eng.*, vol. 8, pp. 63–91, 2006.

[71] W. Lionheart, "Review: Developments in EIT reconstruction algorithms: Pitfalls, challenges and recent developments," *Physiol. Meas.*, vol. 25, pp. 125–142, 2004.

[72] L. Mello, E. Sturler, G. Paulino, and E. Silva, "Recycling Krylov subspaces for efficient large-scale electrical impedance tomography," *Comput. Methods Appl. Mech. Eng.*, vol. 199, pp. 3101–3110, 2010.

[73] T. Bera, S. Biswas, K. Rajan, and J. Nagaraju, "Improving image quality in electrical impedance tomography (EIT) using projection error propagation-based regularization (PEPR) technique: A simulation study," *J. Electr. Bioimp*, vol. 2, pp. 2–12, 2011.

[74] A. Malich, T. Böhm, M. Facius, M. Freessmeyer, M. Fleck, R. Anderson, and W. Kaiser, "Additional value of electrical impedance scanning: Experience of 240 histologically-proven breast lesions," *Eur. J. Cancer*, vol. 37, no. 18, pp. 2324–2330, 2001.

[75] J. da Silva, J. de Sá, and J. Jossinet, "Classification of breast tissue by electrical impedance spectroscopy," *Med. Biol. Eng. Comput.*, vol. 38, no. 1, pp. 26–30, 2000.

[76] A. Stojadinovic, A. Nissan, Z. Gallimidi, S. Lenington, W. Logan, M. Zuley, A. Yeshaya, M. Shimonov, M. Melloul, S. Fields, T. Allweis, R. Ginor, D. Gur, and C. Shriver, "Electrical impedance scanning for the early detection of breast cancer in young women: Preliminary results of a multicenter prospective clinical trial," *J. Clinical Oncol.*, vol. 23, no. 12, pp. 2703–2715, Apr. 2005.

[77] N. Houssami, L. Irwig, J. M. Simpson, M. McKessar, S. Blome, and J. Noakes, "Sydney breast imaging accuracy study: Comparative sensitivity and specificity of mammography and sonography in young women with symptoms," *AJR Am. J. Roentgenol.*, vol. 180, no. 4, pp. 935–940, Apr. 2003.

[78] A. Stojadinovic, A. Nissan, C. Shriver, E. Mittendorf, M. Akin, V. Dickerson, S. Lenington, L. Platt, T. Stavros, S. Goldstein, O. Moskovitz, Z. Gallimidi, S. Fields, A. Yeshaya, T. Allweis, R. Manassa, I. Pappo, R. Ginor, R. D'Agostino, and D. Gur, "Electrical impedance scanning as a new breast cancer risk stratification tool for young women," *J. Surgical Oncol.*, vol. 97, pp. 112–120, 2008.

[79] A. Corlu, "Multi-Spectral and fluorescence diffuse optical tomography of breast cancer," Ph.D. dissertation, Univ. Pennsylvania, Philadelphia, PA, 2007.

[80] S. Konecky, "Non-Invasive imaging of breast cancer with diffusing near-infrared light," Ph.D. dissertation, Univ. Pennsylvania, Philadelphia, PA, 2007.

[81] V. Ntziachristos, A. Yodh, M. Schnall, and B. Chance, "Concurrent MRI and diffuse optical tomography of breast after indocyanine green enhancement," *Proc. Nat. Acad. Sciences USA*, vol. 97, pp. 2767–2772, 2000.

[82] D. Segelstein, "The complex refractive index of water," M.S. thesis, Univ. Missouri, Kansas City, MO, 1981.

[83] R. van Veen, H. Sterenborg, A. Pifferi, A. Torricelli, and R. Cubeddu, "Determination of VIS-NIR absorption coefficients of mammalian fat, with time- and spatially resolved diffuse reflectance and transmission spectroscopy," in *Proc. OSA Annu. Biomed Topical Meeting*, 2004.

[84] S. Prahl, Optical absorption of hemoglobin [Online]. Available: http://omlc.ogi.edu/spectra/hemoglobin 1999

[85] S. van de Ven, S. Elias, A. Wiethoff, M. van der Voort, A. Leproux, T. Nielsen, B. Brendel, L. Bakker, M. van der Mark, W. Mali, and P. Luijten, "Diffuse optical tomography of the breast: Initial validation in benign cysts," *Mol. Imaging Biol.*, vol. 11, no. 2, pp. 64–70, 2009.

[86] R. Choe, S. D. Konecky, A. Corlu, K. Lee, T. Durduran, D. Busch, S. Pathak, B. Czerniecki, J. Tchou, D. Fraker, A. DeMichele, B. Chance, S. Arridge, M. Schweiger, J. Culver, M. Schnall, M. Putt, M. Rosen, and A. Yodh, "Differentiation of benign and malignant breast tumors by *in-vivo* three-dimensional parallel-plate diffuse optical tomography," *J. Biomed. Opt.*, vol. 14, no. 2, p. 024020, 2009.

[87] B. Pogue, S. Poplack, T. McBride, W. Wells, K. Osterman, U. Osterberg, and K. Paulsen, "Quantitative hemoglobin tomography with diffuse near-infrared spectroscopy: Pilot results in the breast," *Radiology*, vol. 218, no. 1, pp. 261–266, 2001.

[88] Safety of laser products—Part 1: Equipment classification and requirements IEC 60825-1 Ed. 2.0 b:2007, 2007.

[89] J. Culver, R. Choe, M. Holboke, L. Zubkov, T. Durduran, A. Slemp, V. Ntziachristos, B. Chance, and A. Yodh, "Three-dimensional diffuse optical tomography in the parallel plane transmission geometry: Evaluation of a hybrid frequency domain/continuous wave clinical system for breast imaging," *Med. Phys.*, vol. 30, no. 2, pp. 235–247, 2003.

[90] B. Brooksby, S. Jiang, H. Dehghani, B. Pogue, K. Paulsen, J. Weaver, C. Kogel, and S. Poplack, "Combining near-infrared tomography and magnetic resonance imaging to study *in vivo* breast tissue: Implementation of a Laplacian-type regularization to incorporate magnetic resonance structure," *J. Biomed Opt.*, vol. 10, no. 5, p. 051504, 2005.

[91] B. Brooksby, B. Pogue, S. Jiang, H. Dehghani, S. Srinivasan, C. Kogel, T. Tosteson, J. Weaver, S. Poplack, and K. Paulsen, "Imaging breast adipose and fibroglandular tissue molecular signatures by using hybrid MRI-guided near-infrared spectral tomography," *Proc. Nat. Acad. Sci. USA*, vol. 103, no. 23, pp. 8828–8833, 2006.

[92] C. Carpenter, B. Pogue, S. Jiang, H. Dehghani, X. Wang, K. Paulsen, W. Wells, J. Forero, C. Kogel, J. Weaver, S. Poplack, and P. Kaufman, "Image-guided optical spectroscopy provides molecular-specific information *in vivo*: MRI-guided spectroscopy of breast cancer hemoglobin, water, and scatterer size," *Opt. Lett.*, vol. 32, no. 8, pp. 933–935, 2007.

[93] F. Bevilacqua, A. Berger, A. Cerussi, D. Jakubowski, and B. Tromberg, "Broadband absorption spectroscopy in turbid media by combined frequency-domain and steady-state methods," *Appl. Opt.*, vol. 39, no. 34, pp. 6498–6507, Dec. 2000.

[94] B. Tromberg, B. Pogue, K. Paulsen, A. Yodh, D. Boas, and A. Cerussi, "Assessing the future of diffuse optical imaging technologies for breast cancer management," *Med. Phys.*, vol. 35, pp. 2443–2451, 2008.

[95] B. Pogue, M. Testorf, T. McBride, U. Osterberg, and K. Paulsen, "Instrumentation and design of a frequency-domain diffuse optical tomography imager for breast cancer detection," *Opt. Expr.*, vol. 1, pp. 391–403, 1997.

[96] X. Intes, "Time-domain optical mammography SoftScan: Initial results," *Acad. Radiol.*, vol. 12, no. 8, pp. 934–947, 2005.

[97] A. Gibson, J. Hebden, and S. Arridge, "Recent advances in diffuse optical imaging," *Phys. Med. Biol.*, vol. 50, pp. R1–R43, 2005.

[98] J. Elisee, A. Gibson, and S. Arridge, "Combination of boundary element method and finite element method in diffuse optical tomography," *IEEE Trans. Biomed. Eng.*, vol. 57, no. 11, pp. 2737–2745, Nov. 2010.

[99] R. Jagannath and P. Yalavarthy, "Approximation of internal refractive index variation improves image guided diffuse optical tomography of breast," *IEEE Trans. Biomed. Eng.*, vol. 57, no. 10, pp. 2560–2563, Oct. 2010.

[100] H. Soliman, A. Gunasekara, M. Rycroft, J. Zubovits, R. Dent, J. Spayne, M. Yaffe, and G. Czarnota, "Functional imaging using diffuse optical spectroscopy of neoadjuvant chemotherapy response in women with locally advanced breast cancer," *Clin. Cancer Res.*, vol. 16, no. 9, pp. 2605–2614, 2010.

[101] B. Tromberg and A. Cerussi, "Imaging breast cancer chemotherapy response with light. Commentary on Soliman *et al*., p. 2605," *Clin. Cancer Res.*, no. 9, pp. 2486–2488, 2010, pp. 16.

[102] A. Cerussi, V. Tanamai, R. Mehta, D. Hsiang, J. Butler, and B. Tromberg, "Frequent optical imaging during breast cancer neoadjuvant chemotherapy reveals dynamic tumor physiology in an individual patient," *Academic Radiol.*, vol. 17, no. 8, pp. 1031–1039, 2010.

[103] S. van de Ven, A. Wiethoff, T. Nielsen, B. Brendel, M. van der Voort, R. Nachabe, M. Van der Mark, M. Van Beek, L. Bakker, L. Fels, S. Elias, P. Luijten, and W. Mali, "A novel fluorescent imaging agent for diffuse optical tomography of the breast: First clinical experience in patients," *Mol. Imaging Biol.*, vol. 12, no. 3, pp. 343–348, 2009.

[104] S. van de Ven, N. Mincu, J. Brunette, G. Ma, M. Khayat, D. Ikeda, and S. Gambhir, "Molecular imaging using light-absorbing imaging agents and a clinical optical breast imaging system—A phantom study," *Mol. Imaging Biol.*, vol. 13, no. 2, pp. 232–238, 2011.

[105] K. Carr, "Microwave radiometry: Its importance to the detection of cancer," *IEEE Trans. Microw. Theory Techn.*, vol. 37, no. 12, pp. 1862–1869, Dec. 1989.

[106] F. Bardati and S. Iudicello, "Modeling the visibility of breast malignancy by a microwave radiometer," *IEEE Trans. Biomed. Eng.*, vol. 55, no. 1, pp. 214–221, Jan. 2008.

[107] S. Jacobsen and Ø. Klemetsen, "Improved detectability in medical microwave radio-thermometers as obtained by active antennas," *IEEE Trans. Biomed. Eng.*, vol. 55, no. 12, pp. 2778–2785, Dec. 2008.

[108] S. Iudicello and F. Bardati, "Functional imaging of compressed breast by microwave radiometry," *Appl. Computational Electromagnetics Soc. J.*, vol. 24, no. 1, pp. 64–71, 2009.

[109] S. Jacobsen and Ø. Klemetsen, "Active antennas in medical microwave radiometry," *Electron. Lett.*, vol. 43, no. 11, pp. 606–608, 2007.

[110] M. El-Shenawee, "Numerical assessment of multifrequency microwave radiometry for sensing malignant breast cancer tumor," *Microw. Opt. Technol. Letters*, vol. 36, no. 5, pp. 394–398, Mar. 2003.

[111] K. Carr, P. Cevasco, P. Dunlea, and J. Shaeffer, "Radiometric sensing: An adjuvant to mammography to determine breast biopsy," in *Proc. IEEE MTT-S Int. Microw. Symp. Dig.*, 2000, vol. 2, pp. 929–932.

[112] J. Lee, S. Lee, K. Kim, W. Han, G. Yoon, L. Pasmanik, I. Ulyanichev, and A. Troitsky, "Experimental investigation of the mammary gland tumour phantom for multifrequency microwave radio-thermometers," *Med. Biological Eng. Computing*, vol. 42, pp. 581–590, 2004.

[113] B. Weiss, G. Ganepola, H. Freeman, Y. Hsu, and M. Faupel, "Surface electrical potentials as a new modality in the diagnosis of breast lesions—A preliminary report," *Breast Disease*, vol. 7, no. 2, pp. 91–98, 1994.

[114] A. Marino, D. Morris, M. Schwalke, I. Iliev, and S. Rogers, "Electrical potential measurements in human breast cancer and benign lesions," *Tumor Biol.*, vol. 15, pp. 147–152, 1994.

[115] M. Faupel, D. Vanel, V. Barth, R. Davies, I. Fentiman, R. Holland, J. Lamarque, V. Sacchini, and I. Schreer, "Electropotential evaluation as a new technique for diagnosing breast lesions," *Eur. J. Radiol.*, vol. 24, no. 1, pp. 33–38, Jan. 1997.

[116] M. Fukuda, K. Shimizu, N. Okamoto, and T. Arimura *et al.*, "Prospective evaluation of skin surface electropotentials in Japanese patients with suspicious breast lesions," *Jpn. J. Cancer Res.*, vol. 87, no. 10, pp. 1092–1096, Oct. 1996.

[117] J. Cuzick, R. Holland, V. Barth, R. Davies, M. Faupel, I. Fentiman, H. Frischbier, J. LaMarque, M. Merson, V. Sacchini, D. Vanel, and U. Veronesi, "Electropotential measurements as a new diagnostic modality for breast cancer," *Lancet*, vol. 352, Aug. 1998.

[118] S. Vinitha Sree, E. Ng, G. Kaw, R. Acharya-U, and B. Chong, "The use of skin surface electropotentials for breast cancer detection—Preliminary clinical trial results obtained using the biofield diagnostic system," *J. Med. Syst.*, vol. 35, no. 1, pp. 79–86, Feb. 2011.
[119] V. Subbhuraam, E. Ng, G. Kaw, R. Acharya, and B. Chong, "Evaluation of the efficiency of biofield diagnostic system in breast cancer detection using clinical study results and classifiers," *J. Med. Syst.* 2010 [Online]. Available: http://www.springerlink.com/content/fr76235441425447/, (in press)
[120] M. Faupel, B. Barrett, J. Stephens, and S. Nathanson, "D.C. biopotential sensing electrode and electroconductive medium for use therein," U.S. Patent 5,823,957, Oct. 20, 1998.
[121] [Online]. Available: http://www.mackaylifesciences.com/v2/
[122] S. Vinitha Sree, E. Y. K. Ng, and U. Rajendra Acharya, "Data mining approach to evaluating the use of skin surface electropotentials for breast cancer detection," *Technol. Cancer Res. Treatment*, vol. 9, no. 1, pp. 95–106, 2010.
[123] A. Hassan and M. El-Shenawee, "Modeling electrical activities of a growing breast cancerous cell based on a semiconductor approach," in *Proc. 31st Annu. Int. Conf. IEEE Eng. Medicine Biology Soc.*, Minneapolis, MN, Sep. 2–6, 2009, pp. 3905–3908.
[124] A. Hassan and M. El-Shenawee, "Diffusion-drift modeling of a growing breast cancerous cell," *IEEE Trans. Biomed. Eng.*, vol. 56, no. 10, pp. 2370–2379, Oct. 2009.
[125] A. Hassan and M. El-Shenawee, "Modeling electromagnetic signals of multiple breast cancerous cells," in *Proc. URSI Nat. Radio Sci. Meeting*, Boulder, CO, Jan. 6–9, 2010.
[126] A. Hassan and M. El-Shenawee, "Modeling biopotential signals and current densities of multiple breast cancerous cells," *IEEE Trans. Biomed. Eng.*, vol. 57, no. 9, pp. 2099–2106, Sep. 2010.
[127] A. Hassan and M. El-Shenawee, "The MPI parallelization of the diffusion-drift algorithm for quantitative analysis of breast tumor electric signals," in *Proc. IEEE Int. Symp. Antennas Propagation USNC/URSI Nat. Radio Sci. Meeting*, Toronto, Canada, Jul. 11–17, 2010.
[128] A. Hassan and M. El-Shenawee, "Parallel implementation of the diffusion-drift algorithm for modeling the electrophysiological activity of breast tumors," *J. Parallel Distributed Computing*, vol. 71, no. 7, pp. 1011–1023, 2011.
[129] A. Hassan, "The diffusion-drift algorithm for modeling the biopotential signals of breast cancer tumors," Ph.D. dissertation, Univ. Arkansas, Fayetteville, Dec. 2010.
[130] P. Anninos, A. Kotini, N. Koutlaki, A. Adamopouos, G. Galazios, and P. Anastasiadis, "Differential diagnosis of breast lesions by use of biomagnetic activity and non-linear analysis," *Eur. J. Gynaecolog. Oncol.*, vol. 21, no. 6, pp. 591–595, 2000.
[131] A. Kotini, A. Anastasiadis, N. Koutlaki, D. Tamiolakis, P. Anninos, and P. Anastiadis, "Biomagnetism in gynaecologic oncology. Our experience in Greece," *Eur. J. Gynaecol. Oncol.*, vol. 27, no. 6, pp. 594–596, 2006.
[132] P. Anastasiadis, P. Anninos, and E. Sivridis, "Biomagnetic activity in breast lesions," *Breast*, vol. 3, pp. 177–180, 1994.
[133] S. Baillet, J. Mosher, and R. Leahy, "Electromagnetic brain mapping," *IEEE Signal Processing Mag.*, vol. 18, no. 6, pp. 14–30, 2001.
[134] P. C. Lauterbur, "Image formation by induced local interactions: Examples employing nuclear magnetic resonance," *Nature*, vol. 242, pp. 190–191, March 1973.
[135] M. A. Brown and R. C. Semelka, *MRI: Basic Principles Applicat.*, 3rd ed. New York: Wiley, 2003.
[136] S. Harms, "MRI in breast cancer diagnosis and treatment," *Curr. Probl. Diagn. Radiol.*, vol. 25, no. 6, pp. 193–215, 1996.
[137] D. Ikeda, D. Baker, and B. Daniel, "Magnetic resonance imaging of breast cancer: Clinical indications and breast MRI reporting system," *J. Magn. Reson. Imaging*, vol. 12, no. 6, pp. 975–983, 2000.
[138] D. Koh and A. Padhani, "Diffusion-weighted MRI: A new functional clinical technique for tumour imaging," *Brit. J. Radiol.*, vol. 79, pp. 633–635, 2006.
[139] M. Iima, D. Le Bihan, R. Okumura, T. Okada, K. Fujimoto, S. Kanao, S. Tanaka, M. Fujimoto, H. Sakashita, and K. Togashi, "Apparent diffusion coefficient as an MR imaging biomarker of low-risk ductal carcinoma *in situ*: A pilot study," *Radiology*, vol. 260, no. 2, pp. 364–372, 2011.
[140] H. Rahbar, S. Partridge, P. Eby, W. Demartini, R. Gutierrez, S. Peacock, and C. Lehman, "Characterization of ductal carcinoma *in situ* on diffusion weighted breast MRI," *Eur. Radiol.*, vol. 21, no. 9, pp. 2011–2019, 2011.
[141] M. Kriege, C. Brekelmans, C. Boetes, and P. Besnard *et al.*, "Efficacy of MRI and mammography for breast-cancer screening in women with a familial or genetic predisposition," *N. Engl. J. Med.*, vol. 351, no. 5, pp. 427–437, 2004.
[142] C. Kuhl, S. Schrading, C. Leutner, N. Morakkabati-Spitz, E. Wardelmann, R. Fimmers, W. Kuhn, and H. Schild, "Mammography, breast ultrasound, and magnetic resonance imaging for surveillance of women at high familial risk for breast cancer," *J. Clin. Oncol.*, vol. 23, no. 33, pp. 8469–8476, 2005.
[143] L. Esserman, N. Hylton, L. Yassa, J. Barclay, S. Frankel, and E. Sickles, "Utility of magnetic resonance imaging in the management of breast cancer: Evidence for improved preoperative staging," *J. Clin. Oncol.*, vol. 17, pp. 110–119, 1999.
[144] J. Menell, E. Morris, D. Dershaw, A. Abramson, E. Brogi, and L. Liberman, "Determination of the presence and extent of pure ductal carcinoma *in situ* by mammography and magnetic resonance imaging," *Breast J.*, vol. 11, no. 6, pp. 382–390, 2005.
[145] C. Kuhl, S. Schrading, H. Bieling, E. Wardelmann, C. Leutner, R. Koenig, W. Kuhn, and H. Schild, "MRI for diagnosis of pure ductal carcinoma *in situ*: A prospective observational study," *Lancet*, vol. 370, pp. 485–492, 2007.
[146] N. Tsuboi, Y. Ogawa, T. Inomata, D. Yoshida, S. Yoshida, and T. Moriki *et al.*, "Changes in the findings of dynamic MRI by preoperative CAF chemotherapy for patients with breast cancer of stage II and III: Pathologic correlation," *Oncol. Rep.*, vol. 6, pp. 727–732, 1999.
[147] R. Warren, "Is breast MRI mature enough to be recommended for general use?," *Lancet*, vol. 358, no. 9295, pp. 1745–1746, 2001.
[148] K. Gundry, "The application of breast MRI in staging and screening for breast cancer," *Oncology (Williston Park)*, vol. 19, no. 2, pp. 159–169, 2005.

Ahmed M. Hassan (S'07) received the B.Sc. degree (with highest honors) and the M.Sc. degree both in electronics and communications engineering from Cairo University, Cairo, Egypt, in 2004 and 2006, respectively. He received the Ph.D. degree in electrical engineering in modeling the bioelectromagnetics of breast cancer from the University of Arkansas, Fayetteville, in 2010.

From 2004 to 2006, he was a Teaching Assistant at Cairo University, where he was also an Assistant Lecturer during 2006. From 2007 to 2010, he was a Teaching and Research Assistant in the Department of Electrical Engineering at the University of Arkansas. Currently, he is a Postdoctoral Fellow in the Department of Electrical Engineering, University of Arkansas. His current research interests include bioelectromagnetics, modeling of the electrical activities of cancerous cells, biophysics, metamaterials, experimental microwave imaging, and terahertz imaging.

Dr. Hassan is the recipient of the Doctoral Academy Fellowship at the University of Arkansas.

Magda El-Shenawee (M'91–SM'02) received the Ph.D. degree in electrical engineering from the University of Nebraska-Lincoln, Lincoln, in 1991.

She was a Research Associate at the Center for Electro-Optics, University of Nebraska-Lincoln during 1992 to 1994, where she was involved in the research on the enhanced backscatter phenomenon from random rough ground surfaces. She was involved in research at the National Research Center, Cairo, Egypt, during 1994 to 1996, and at the University of Illinois, Urbana-Champaign, during 1997 through 1999. During 1999 through 2001, she was a Member of the Multidisciplinary University Research Initiative team, Northeastern University, Boston, MA, where she was involved in the research on the antipersonnel landmine detection. She joined the University of Arkansas, Fayetteville, as an Assistant Professor in 2001, where she is currently a Professor of electrical engineering. Her research interests include inverse scattering algorithms, terahertz imaging of biological tissue, computational electromagnetics, biomedical engineering application to breast cancer research using biopotentials, biomagnetics, biological tumor growth modeling, and microwave imaging algorithms of breast cancer.

Dr. El-Shenawee is a member of Eta Kappa Nu electrical engineering honor society.